

5-2015

# Novel methodologies to study protein S-glutathiolation using fluorescence spectroscopy

Jacob Daniels
*College of William and Mary*

Novel methodologies to study protein S-glutathiolation using fluorescence spectroscopy

A thesis submitted in partial fulfillment of the requirement
for the degree of Bachelor of Science in Chemistry from
The College of William and Mary

by

Jacob Donald Daniels

Accepted for _____

_____
Lisa M. Landino, Director

_____
Christopher J. Abelt

_____
Gary W. Rice

_____
Pamela S. Hunt

Williamsburg, VA
May 6, 2015

# Table of Contents

# Abstract

Protein oxidation and repair is a physiological process that has been implicated in the pathology of diseases such as Alzheimer's and in the normal aging process. S-glutathiolation, the process by which glutathione reacts at equilibrium with a protein and prevents the protein from undergoing further oxidation, is a critical repair mechanism for oxidized proteins.

In this thesis, we use the technique of fluorescence spectroscopy to develop a methodology to visualize S-glutathiolation *in vitro*. We report the spectroscopic properties of previously synthesized glutathione derivatives that have successfully labeled proteins during periods of oxidation. We also report the results of labeling BSA and papain, two proteins that contain one cysteine, at their cysteine and amine residues as well as the effect of unfolding on the dansyl emission wavelength for the cysteine-labeled proteins. In addition, we report the emission wavelengths from four proteins: BSA, papain, CK, and GAPDH, labeled with D-GSH in the presence of $H_2O_2$.

The results from the experiments herein demonstrate the usefulness of this methodology. Oxidative labeling of proteins with D-GSH results in an emission wavelength that varies between proteins and is lower than the D-GSH emission wavelength. While this proves to be a promising result, the model is only tested with proteins containing up to four cysteines and the labeling mechanism for multi-cysteine proteins is not currently understood. Further refinement is required before implementation.

# Chemical Index

Sodium phosphate buffer (PB)

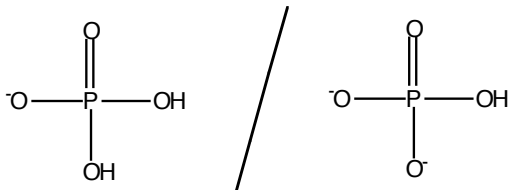

$H_2PO_4^-$ $HPO_4^{2-}$

Tris(hydroxymethyl)aminomethane (Tris)

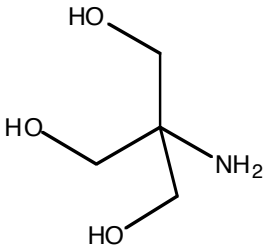

GSH

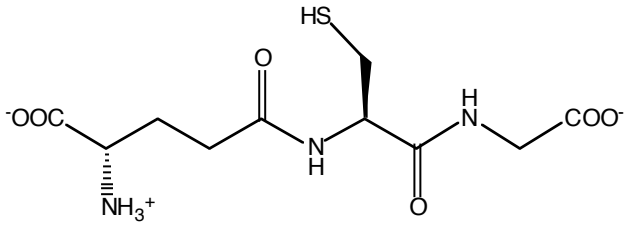

GSSG

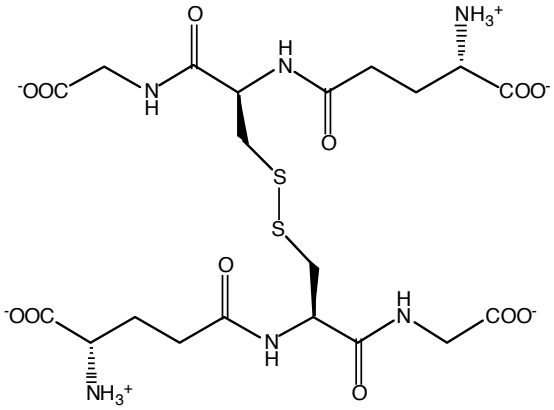

Dansyl chloride

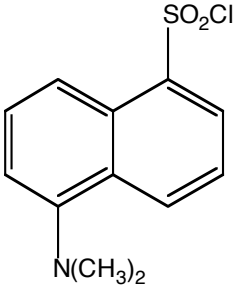

IDANS

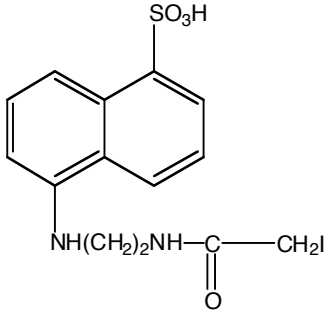

Fluorescein isothiocyanate (FITC)

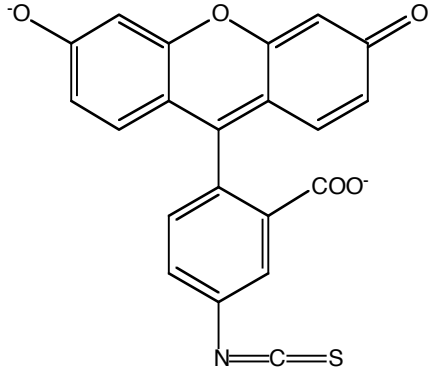

Iodoacetamide fluorescein (IAF)

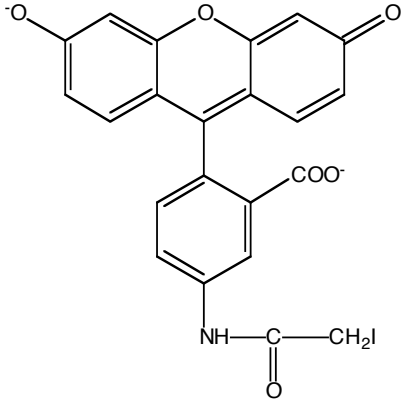

Dansyl glycine (DG)

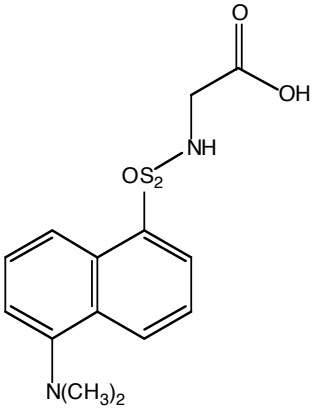

Dansyl acid

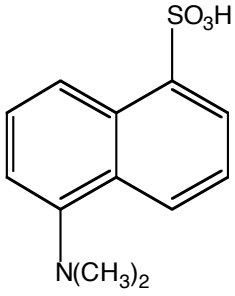

D-GSH

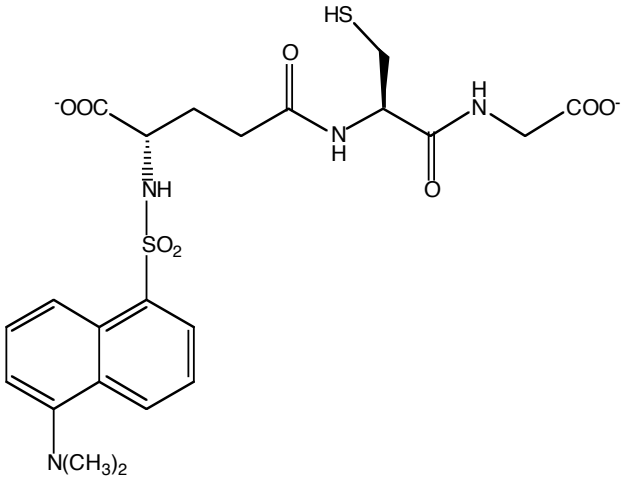

GS-DANS

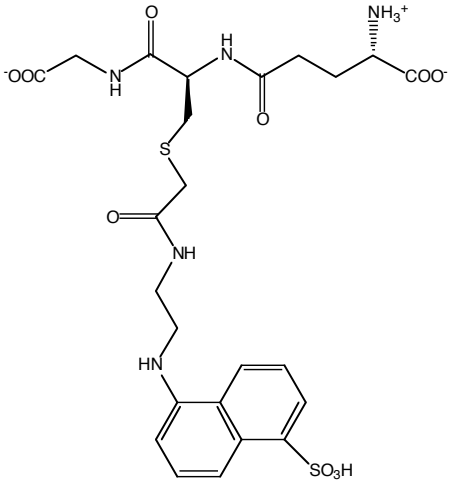

D-GSSG (D1)

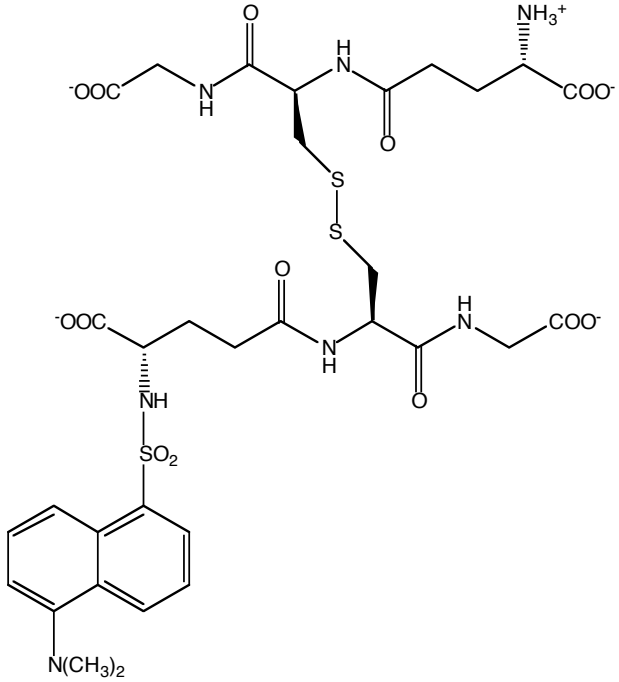

D-GSSG-D (D2)

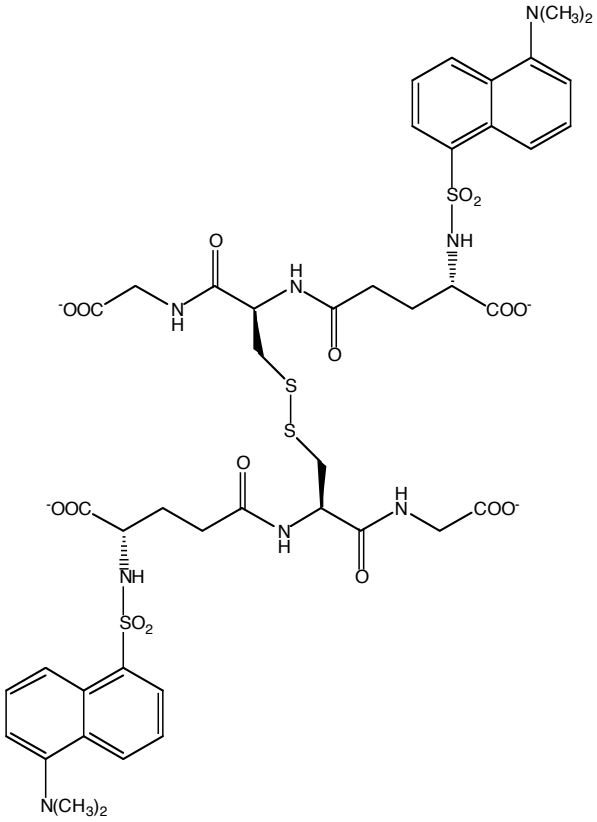

F-GSH

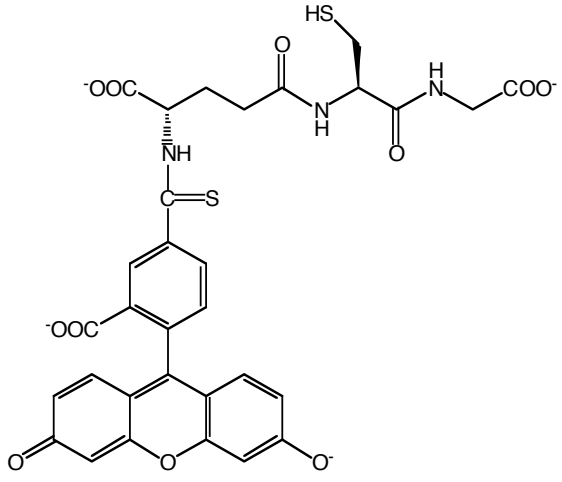

F-GSSG (F1)

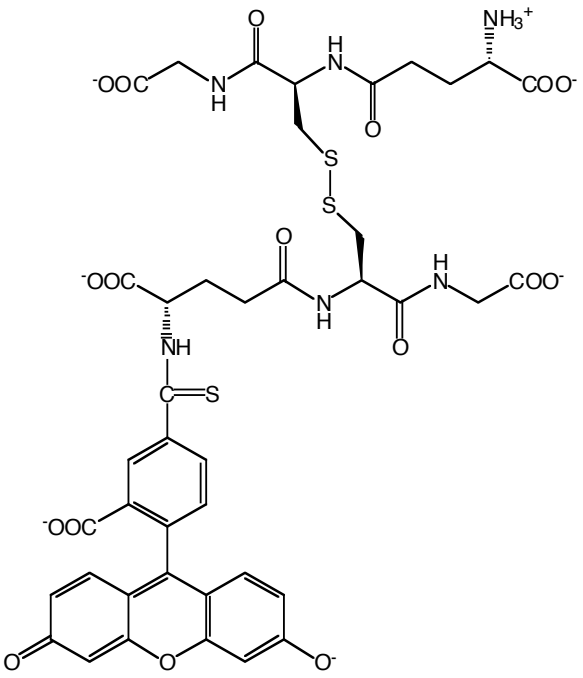

F-GSSG-F (F2)

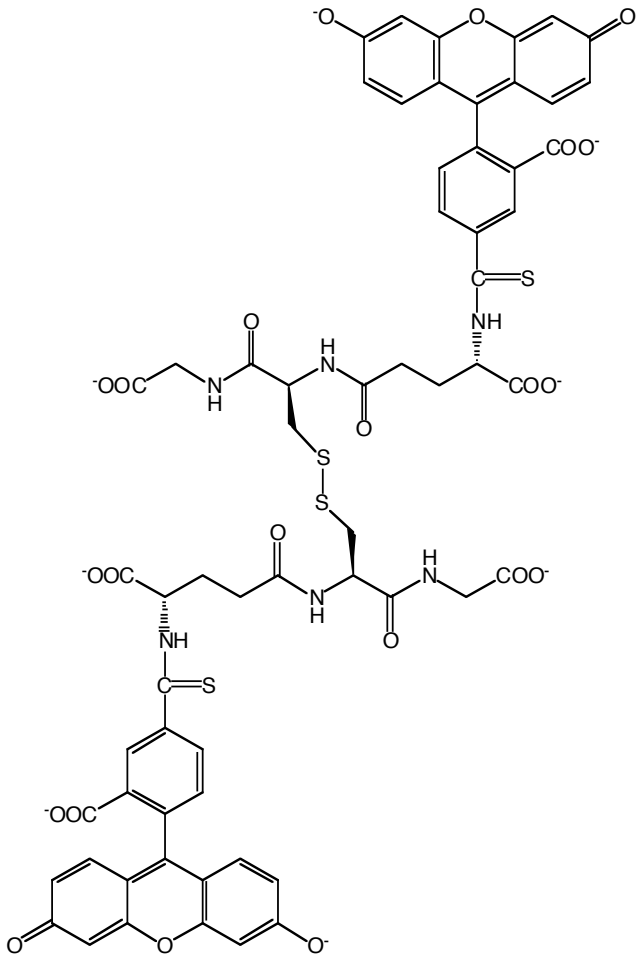

Dithiothreitol (DTT)

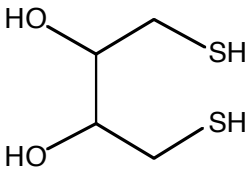

Tris(2-carboxyethyl)phosphine hydrochloride (TCEP)

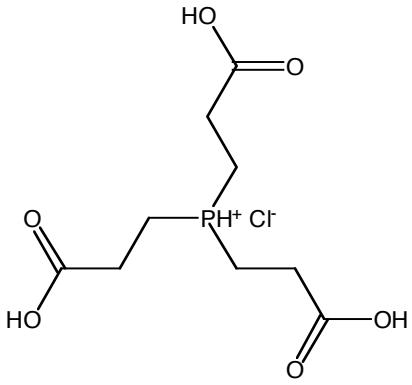

Guanidine hydrochloride (guHCl)

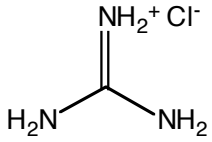


Iodoacetamide (IAM)

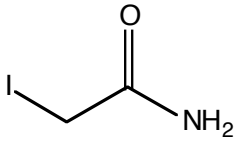


**Reagents**

- Acetic Acid (HAc)
- Acetone
- Acetonitrile (AcCN)
- Ammonium bicarbonate
- Bicinchoninic acid (BCA)
- Dimethylformamide (DMF)
- Ethanol (EtOH)
- Methanol (MeOH)
- Sodium bicarbonate
- Sodium dodecyl sulfate (SDS)

**Proteins:**

- Bovine serum albumin (BSA)
- Creatine kinase (CK)
- Glyceraldehyde-3-phosphate dehydrogenase (GAPDH)
- papain

# Table of Figures

# Introduction

### A: The use of fluorescence in Biochemistry

Fluorescence remains a critical tool in the fields of biochemistry and molecular biology. The development of both fields, in particular, has relied upon fluorescence to aid in the study of the underlying chemical processes of life. As of March 2015, a cursory search on PubMed using the terms 'Fluorescence' and 'Biochemistry' will yield 337 results from the year 2015 alone and a similar search using the term 'GFP' yields 714 results during the same period. Fluorescence is an ideal tool to study biochemistry, because it is sensitive, specific, and, most importantly for *in vivo* experiments, non-invasive [1]. The inherent sensitivity of fluorescence allows it to be applied in a wide range of experimental designs, ranging from a single molecule all the way to an entire organism, as is the case with ANDi and Mr. Green Genes, a fluorescent monkey and cat, respectively [2].

Originally biochemists were limited in their use of fluorescence, only being able to attach small organic dyes to molecules of interest through the means of antibody recognition [2]. While this technique provided numerous insights, it also had numerous drawbacks. First, use of antibodies, while selective, requires an understanding of the molecule of interest to generate an antibody to target it. Second, antibodies have both specific and non-specific binding and third, this technique requires that cells be fixed and permeabilized, preventing live imaging techniques [2]. Despite these drawbacks, fluorescent labeling using antibodies is still a widely used technique within biochemistry. This technique, called immunofluorescence, allows for the visualization of cellular components, such as in [3], where immunofluorescence is used to visualize newly generated neurons in the dentate gyrus following a drug treatment, or in [4],

where immunofluorescence is used to visualize chromatin structure and how it is affected by the inhibition of glycolysis.

Many of the experimental limitations of immunofluorescence were removed when new technological advances allowed for a fluorophore to directly label a molecule of interest. Importantly, this advancement allows for live imaging of cells and cellular components [2]. However, this technique, like immunofluorescence, requires an understanding of the target molecule in order to design a fluorophore that will selectively label it. Despite this limitation, this method of labeling is widely used, from labeling intracellular proteins tagged with histidine [5], to the use of fluorescent in situ hybridization (FISH) to detect chromosomal mutations in an individual suffering from a sexual development disorder [6], or to detect RNA within tumor cells [7].

By far, one of the most impactful findings in the field of biochemistry has been the discovery and isolation of Green Fluorescent Protein (GFP) from the *Aequorea victoria* jellyfish, a discovery that won the 2008 Nobel Prize in Chemistry. GFP, which is intrinsically fluorescent requiring no cofactors or substrates, emits green light when excited with blue light [8]. The fluorescence of GFP results from the formation of the chromophore from three amino acid side chains, ser65, tyr66, and gly67, via an autocatalytic cyclization reaction [8,9]. This chromophore is found in the center of the β barrel structure that comprises the structure of GFP, largely shielding it from the exterior environment [8]. Since its initial discovery, the spectroscopic properties of GFP have readily been characterized. GFP absorbs predominantly at two wavelengths, with a major peak at 398nm and a minor peak at 475nm [8]. Excitation at 398nm results in an emission maximum at 508nm and excitation at 475nm results in an emission maximum at 503nm. [8]

The use of GFP as a fluorophore provides almost limitless possibilities. GFP is a highly stable molecule resistant to heat, alkalinity, pH, detergents, photobleaching, salts, and proteases, allowing it to be used in a wide range of cellular conditions [8]. In addition, GFP is nontoxic to most cells, preventing deleterious side reactions [8]. As GFP is a protein with a known sequence, it can be easily expressed by cells without having to cross the plasma membrane [8]. Most importantly, with the advent of genetic manipulation, the sequence of GFP can be added to any known protein sequence, which when translated, results in a protein containing a GFP tag [8]. It is important to note that the fusion of GFP to a protein has no effect on the function or localization of the protein of interest, ensuring that the fundamental biochemical function is not altered [8]. GFP fusion proteins have a wide range of applications, ranging from the monitoring of gene expression to examining the localization of a protein of interest [8]. In this way, GFP provides a means of noninvasively imaging dynamic cellular events, an application that previous fluorescence methods had been unable to do [8].

Fluorescence is primarily used for one of two experimental designs: detection and imaging or structural elucidation. The sensitivity of fluorescence allows it to measure minute quantities of a substance with good resolution. In conjunction with the new labeling methods described above, the implantation of new techniques, like microscopy and fluorescence resonance energy transfer (FRET), has allowed fluorescence to expand beyond its initially limited conditions [10,11].

Fluorescence is widely used as a means of detection for a wide range of molecules and processes. Due to its overall sensitivity down to a single molecule, fluorescence provides an accurate means of detecting substances in nano and picomolar concentrations. Within the literature there are numerous instances in which fluorescence is employed to detect a desired

analyte or biochemical process. These range from the detection of single molecules like $H_2O_2$ and $H_2S$ [12,13], to the detection and measurement of the activity of enzymes such as uracil-DNA glycosylase and acetycholinesterase [14,15], to the detection of cellular processes like apoptosis [16]. The previous examples provide just five of numerous ways in which fluorescence is used as a means of detection, though they provide a great example of the widespread benefit and applicability of the findings obtained from these studies, ranging from a greater understanding of the pathology of Alzheimer's and Down's Syndrome [12,13], to an increased understanding of the fundamental processes behind life, such as neurotransmission and cell death [13,16].

In addition to detection, fluorescence is widely used as a means of structural elucidation. Two factors make it an especially ideal tool for that application. First, the solvatochromic properties of many fluorophores, where the fluorescence wavelength shifts depending on the environmental conditions, allow one to analyze the environment surrounding a given fluorophore [1]. For a fluorophore attached to a protein, this fact allows a researcher to determine the protein microenvironment at the site of attachment, providing an understanding of both protein composition and folding [1]. Second, new methodologies, such as microscopy and FRET, allow fluorescence to probe previously inaccessible environments. The use of fluorescence for structural elucidation is especially useful when examining proteins. Proteins, due to their large size and 3D structure, present challenges for structural studies. Commonly used biochemical protocols, like sodium dodecyl sulfate polyacrylamide gel electrophoresis (SDS PAGE), while providing a means of assessing the size and mass of a protein, denature proteins, thereby preventing analysis of the 3D structure of a protein. In the same manner, techniques like X-ray crystallography and NMR, which are able to provide structural resolution of proteins, face

numerous experimental complications that prevent them for being applied to study a large portion of proteins. X-ray crystallography requires proteins to be crystallized, which for some proteins like receptors represents a hindrance to study, though new experimental protocols are improving the applicability of this technique; researchers have been able to successfully crystalize the human $GABA_B$ receptor and perform structural studies [17]. NMR, which provides information regarding protein dynamics, faces both size and cost limitations. Currently NMR is limited to a protein size of around 35kD, though new experimental technology and NMR protocols are seeking to extend this limit [18]. These new technologies, however, require electromagnets with high field strength, typically around 800MHz, representing a significant cost limitation.

Current research applying fluorescence for structural elucidation is widely varied. Previous research, before the advent of microscopy techniques, was largely limited to studies of protein folding, as seen with Waldo et al. who devised an assay to rapidly detect protein folding in *E. coli* using GFP [19]. Recently developed spectroscopic techniques have allowed the scope of fluorescence studies beyond protein folding, such as the study of membrane composition and structure through fluorescence correlation spectroscopy, where fluctuations in the fluorescence signal can be used to calculate diffusion constants and concentrations for membrane structures [20]. The application of FRET to biological processes has allowed researchers to study a wide range of topics beyond protein folding. One such example is the study of electrostatic lipid-protein interactions [21], as well as the study of the RNA structure of structures underlying influenza infection, with implications for anti-viral drug design [22]. Microscopy techniques have allowed structural studies to expand widely in scope and in greater detail. One such example is the use of single-molecule microscopy to study interactions of the Amyloid-β 42

(Aβ42) peptide with membranes as a means of better understanding the disease pathology of Alzheimer's [23]. In addition, microscopy techniques have allowed researchers to perform *in vivo* live imagining experiments of dynamic cellular events, such as actin filament growth and branching [24], providing greater knowledge of cytoskeletal structure. As detailed in [25], combining FRET and microscopy in a technique called FRET microscopy, has allowed researchers to study, among other processes, interactions between proteins as well as providing a means of examining protein folding *in vivo*. Since its advent, FRET microscopy expanded beyond protein folding and has allowed researchers to study cellular events like exocytosis and vesicle fusion [26], as well as the activity and function of receptors [27].

As detailed above, the use of fluorescence in biochemistry has allowed researchers to study a wide variety of biological processes with implications ranging from drug design to understanding disease pathology. This can and will only increase. New technologies, such as the development of new fluorescent probes, targeting strategies, and instrumentation and techniques, have greatly increased the applicability of fluorescence to study biochemical processes [2]. One such process, protein oxidation and repair, is an active feature of study in the Landino laboratory.

**B. Protein oxidation and S-glutathiolation**

Humans, as aerobic organisms, are subject to the formation of reactive oxygen species (ROS) as a result of oxygen turnover in cells. In addition, ROS are endogenous and function in normal cellular processes like signaling and division [28]. While part of normal cellular functions, ROS can have deleterious effects due to their ability to modify the redox balance within cells. In this modification of the redox balance, ROS and their nitrogen counterparts (RNS) cause specific oxidative modifications to proteins [29]. These modifications, both reversible and irreversible in nature, result from the modification of critical amino acid side

chains within a protein, affecting, often negatively, the activity and function of the oxidized proteins [28,29]. Cysteine, a critical amino acid within numerous proteins, is especially susceptible to oxidative modification due to the reactive thiol (RSH) within its side chain [29]. Oxidation of cysteinyl thiols results in the formation of disulfide bonds (RSSR) that can cause protein misfolding and aggregation [29]. As a result of their ability to modify critical proteins within cells, ROS and RNS have been implicated in the pathologies of numerous diseases including Amyotrophic Lateral Sclerosis and Alzheimer's, as well as functioning as part of the normal aging process [28].

While ROS and RNS are detrimental to cells, numerous mechanisms exist that serve to prevent damage. These mechanisms primarily consist of enzymes such as superoxide dismutase (SOD) and low molecular mass redox active molecules like vitamin E, vitamin C, and glutathione (GSH) (Figure 1); a tripeptide composed of L-glutamic acid, L-cysteine, and L-glycine, with a γ-peptide bond linking glutamic acid and cysteine [28]. Within the cell, glutathione exists primarily in two forms based on its oxidation state; when oxidized it is GSSG and when reduced it is GSH. Glutathione is an efficient antioxidant for two primary reasons: 1) both GSH and GSSG are very soluble in aqueous solution [30], and 2) the γ-peptide bond is highly resistant to degradation by intracellular peptidases, making glutathione a stable molecule in a variety of cellular environments [30]. The antioxidant effects of GSH are enhanced by the fact that within the cytosol, the ratio of GSH to GSSG is maintained at levels ranging from 1000:1 and 100:1 [30]. The high concentration of GSH ensures that the majority of cytosolic proteins are reduced, thereby maintaining normal cellular function. Importantly, the oxidation of GSH to GSSG is not permanent; rather GSSG can be reduced to GSH through two primary

mechanisms: thiol/disulfide exchange, and the glutathione reductase system, which uses an NADPH cofactor produced in the pentose phosphate pathway [30].

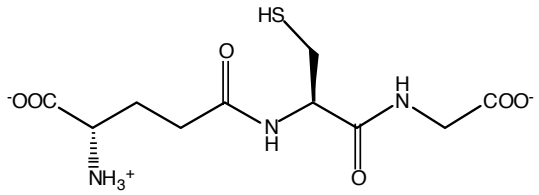


**Figure 1: GSH at physiological pH**

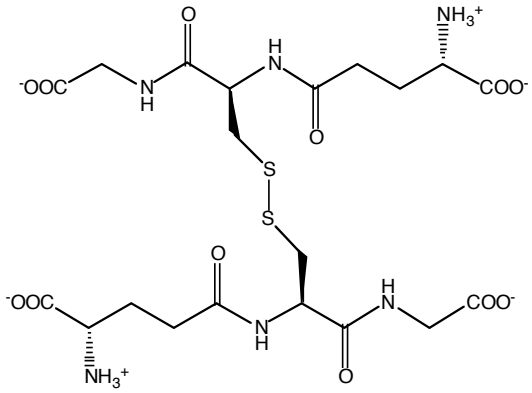


**Figure 2: GSSG at physiological pH**

GSH is especially critical within cells due to its ability to non-enzymatically modify protein thiols (RSH) in a process known as S-glutathiolation. S-glutathiolation is involved in numerous cellular processes, the most critical of which being the protection of protein thiols against irreversible oxidation [28]. S-glutathiolation is especially pronounced during periods of oxidative and nitrosative stress [28]. The primary mechanism by which a protein is glutathiolated is via the oxidation of GSH to GSSG followed by direct thiol-disulfide exchange with the protein thiol [30]. Upon glutathiolation, a protein thiol is no longer susceptible to oxidation, thus preventing permanent protein dysfunction as a result of oxidative stress [29]. S-glutathiolation, while clearly beneficial to proteins, is not a ubiquitous process; rather it is affected by the reactivity and accessibility of the protein thiol and is favored in basic environments [30]. While S-glutathiolation serves to protect proteins from oxidation during oxidative stress it may render proteins inactive, contributing to the overall cellular dysfunction that occurs during periods of oxidative stress [31]. Dethiolation of S-glutathiolated proteins occurs through three primary mechanisms: non-enzymatic reduction, enzymatic cleavage of the disulfide bond by the

glutathione reductase system, or via direct thiol disulfide exchange with GSH after the intracellular redox balance is restored [28,29].

Because of its ability to protect protein thiols, GSH serves as a modulating factor for a number of critical proteins during oxidative and nitrosative stress [31]. One such protein is tubulin, the primary component of microtubules and a major research focus in the lab. [32] Microtubules are critical in normal cellular function as they provide structure to the cell and are involved in both cellular signaling and transport. With roughly fifteen accessible thiols out of twenty total [32], tubulin is oxidized easily *in vitro* during periods of oxidative and nitrosative stress [32-36]; experiments using a mammalian cell line have also shown that tubulin is oxidized *in vivo* [37]. As microtubule formation is dependent on the polymerization of tubulin, oxidation of tubulin results in inhibition of microtubule polymerization and overall microtubular dysfunction [32, 34-38]. While deleterious to the cell, the oxidation of tubulin, and other proteins, is repaired by the glutathione reductase system composed of glutathione reductase, GSH, NADPH, and glutaredoxin [32, 38]. The presence of GSH within the glutathione reductase system is critical in the repair of oxidized tubulin, as oxidized tubulin is able to undergo thiol disulfide exchange with GSH, forming oxidized GSSG and reduced tubulin (Figure 3) [32]. In addition, reduced tubulin undergoes thiol-disulfide exchange with GSSG to produce oxidized tubulin and GSH (Figure 4) [32].

$$\text{tubulin (ox)} + \text{GSH} \rightarrow \text{tubulin (red)} + \text{GSSG}$$

Figure 3: Reduction of tubulin by GSH.

$$\text{tubulin (red)} + \text{GSSG} \rightarrow \text{tubulin (ox)} + \text{GSH}$$

Figure 4: Oxidation of tubulin by GSSG.

Due to tubulin's reactivity with both oxidized and reduced glutathione, we believe that precise cellular control of GSH:GSSG is required to maintain tubulin, and other proteins, in the reduced, functional state. Considering that tubulin accounts for as much as 15% of total cytosolic protein and that GSH is the most abundant nonprotein thiol present in cells, the precise control of GSH:GSSG becomes especially critical [32].

Understanding of the exact role of S-glutathiolation within cells has been limited due to the inability to detect S-glutathiolation *in vivo*. Numerous experimental methods have been developed to detect S-glutathiolation *in vitro*, including HPLC and MS; however, these systems are unable to discern whether the measured Sis simply a product of environmental conditions or an *in vivo* process [28]. The use of fluorescently tagged glutathione provides an ideal method for the detection of S-glutahiolation due to the high sensitivity of fluorescence. Current research in the lab has focused on developing an *in vitro* model of protein oxidation and S-glutathiolation using purified proteins. Two different fluorophores are currently employed in the lab to aid in this study, dansyl and fluorescein.

**C. Spectroscopic properties of dansyl and fluorescein**

Both dansyl and fluorescein are widely used in the labeling of amino acids and proteins, readily available, and well characterized, making them ideal candidates for this study. For each fluorophore, two derivatives are used, each of which reacts with different functional groups, allowing for the selective modification of amino acid side chains.

Fluorescein, one of the most commonly used fluorophores in biochemical research, was the first fluorophore studied in the lab. Fluorescein is an especially ideal fluorophore as it has a high molar absorptivity, a large fluorescence quantum yield (Q) equal to 0.92, in $H_2O$ with minimal variation in different alcohol solvents [39], and has high photostability in a variety of

buffers [39,40]. However, careful consideration must be applied when using fluorescein. Fluorescein contains 3 ionizable groups, which allows it to exist in one of four ionization states depending on net charge; cationic, neutral, anionic, and dianionic [41]. Interconversion between these states is pH dependent; above pH 6.43 fluorescein exists in the dianionic state [41]. Each ionization state of fluorescein exhibits different spectroscopic properties, thus the buffer pH must be carefully controlled when using fluorescein [41]. As all of the experiments in the lab occur above pH 6.43, the information presented hereafter is for the dianionic form ($F^{2-}$).

Two different molecules of fluorescein are currently used in the lab: FITC (fluorescein isothiocyanate) (Figure 5) and IAF (5-iodoacetamidefluorescein) (Figure 6). Both FITC and IAF share the same overall structure, with the only difference between the two molecules being the functional group, which determines the selectivity. FITC, with the isothiocyanate functional group, reacts with amines and thus attaches to peptides or proteins at free lysine residues and at the N-terminus. IAF, with the iodoacetamide functional group, reacts with thiols and labels peptides and proteins at cysteine residues.

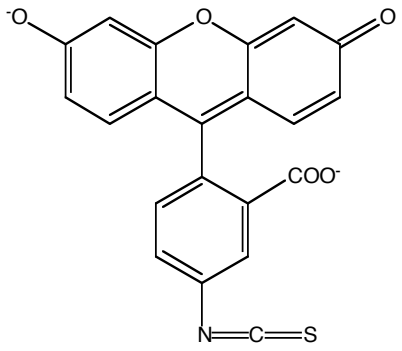


**Figure 5: FITC**

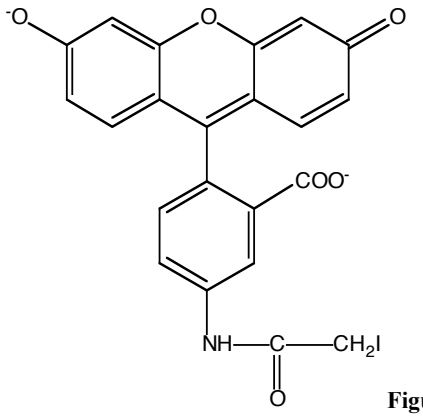


**Figure 6: IAF**

As FITC and IAF share the same overall structure, they also have very similar spectroscopic properties. FITC absorbs at a maximum wavelength of 494 ± 3nm and fluoresces at a maximum wavelength of 520 ± 4nm, while IAF absorbs at a maximum wavelength of 492 ±

3nm and fluoresces at maximum wavelength of 515 ± 4nm [42, 43]. For both FITC and IAF, the above values correspond to measurements in 50mM potassium phosphate pH 9. The dielectric constant for sodium phosphate, D=78.3 debeyes, mirrors that of water, D=78.6 debeyes [44]. For both FITC and IAF, the molar absorptivity constant is especially high at 78,000 ± 7,000 $M^{-1}cm^{-1}$ and 78,000 ± 5,000 $M^{-1}cm^{-1}$, respectively. [42, 43] It is important to note that the phosphate ion is a commonly used buffer within biochemistry, especially for oxidation experiments, as it provides an inert environment in which the reactions can take place; the central phosphate atom is already completely oxidized and is unable to undergo further oxidation.

Additional consideration must be used with fluorescein, as its fluorescence is dependent on two environmental considerations, polarity and protic strength. Fluorescein experiences positive solvatochromism, where as solvent polarity increases, fluorescein undergoes a bathochromic shift to a longer fluorescence wavelength, corresponding to lower energy. [45] This was also observed in aprotic solvents; however, in protic solvents, as the hydrogen bonding power of the solvent increases, the wavelength decreases [45]. These findings are a result of the different properties of the ground and excited states of the fluorescein molecule. The excited state is more polar than the ground state, whereas the ground state has greater hydrogen bond accepting capacity [45]. The quantum yield, however, is minimally affected by solvent polarity: Q= 0.92 in water, Q=0.94 in octanol, Q=0.92 in ethanol [39].

Dansyl, a naphthalene derivative, is another fluorophore used in the lab to study S-glutathiolation. Dansyl is a suitable fluorophore for this purpose because 1) it fluoresces with a high Q in the visible region of the UV/VIS spectrum; 2) it can be attached to proteins and amino acids in a well-understood, high yield reaction; and 3) amino acids that are dansylated are stable

in a broad range of pHs [46]. In addition, the structure of dansyl is not pH–dependent, eliminating one of the experimental considerations of fluorescein.

As for fluorescein, two derivatives of dansyl are used in the lab: dansyl chloride, 5-(dimethylamino)naphthalene-1-sulfonyl chloride, (Figure 7) and IDANS, 5-((((2-iodoacetyl)amino)ethyl)amino)naphthalene-1-sulfonic acid (Figure 8). Both dansyl chloride and IDANS share the same overall structure; both contain the amino naphthalene group with an attached sulfonyl group. The primary structural differences, the sulfonyl chloride in dansyl chloride, and the iodoacetyl group in IDANS, serve as the basis for the selectivity of the molecules. Dansyl chloride is amine–reactive and thus, like FITC, will label lysine residues and the N-terminus of proteins, whereas IDANS, like IAF, is thiol reactive and label cysteine residues.

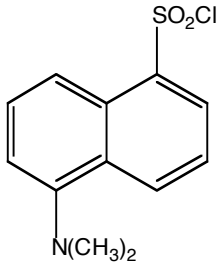


**Figure 7: Dansyl chloride**

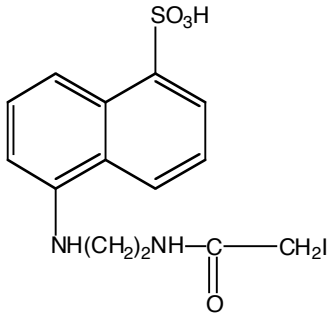


**Figure 8: IDANS**

While dansyl does not display pH dependence, there are still some considerations required when using it, especially for dansyl chloride. Dansyl chloride is not fluorescent until it reacts with an amine. The spectral properties of dansyl are thus dependent on the molecule to which it is attached. For dansyl chloride reacted with n-butylamine, dansyl absorbs at maximum wavelength of 340nm and fluoresces at a maximum wavelength of 510nm [47]. Whereas in chloroform, dansyl n-butylamine absorbs at a maximum wavelength of 341 ± 3nm and fluoresces

at maximum wavelength of 491 ± 4nm with a molar absorptivity of 4700 ± 400$M^{-1}cm^{-1}$ [48]. An understanding of the spectral properties of dansyl amino acids would also be beneficial. Dansyl glycine, the simplest dansyl amino acid, is a widely used dansyl amino acid in labeling experiments. In ethanol, dansyl glycine absorbs at a maximum wavelength of 340nm and fluoresces at a maximum wavelength of 510nm [47]. IDANS shares similar absorption wavelengths with dansyl chloride: 336nm in $H_2O$ and 340nm in ethanol [49]. However, the fluorescence maxima differ greatly from dansyl chloride. IDANS fluoresces at 460nm in EtOH, 452nm in dioxane, and 520nm in $H_2O$ [49]. In addition, the molar absorptivity constant for IDANS differs from dansyl chloride: 5700 ± 400$M^{-1}cm^{-1}$ vs. 4700 ± $M^{-1}cm^{-1}$, respectively [48,50].

The quantum yields, in addition to the molar absorptivity constant and the fluorescence wavelength, differ for dansyl chloride and IDANS. The quantum yield for dansyl tryptophan varies greatly, from Q=0.068 in $H_2O$ to Q=0.70 in dioxane [51]. However, for IDANS, the quantum yield was determined to be 0.54 [52].

Like fluorescein, the fluorescence wavelength for dansyl is dependent on environmental polarity. Both dansyl chloride and IDANS experience positive solvatochromism; the emission wavelength decreases as polarity decreases [49, 51]. However, the relationship is not strictly linear for IDANS. In alcohol solvents beyond 1-butanol, the fluorescence wavelength increases with decreasing solvent polarity [53]. This alcohol effect, however, is not observed for proteins labeled with IDANS; the fluorescence wavelength increases as the protein becomes progressively unfolded, corresponding to an increase in environment polarity [53].

Each of the fluorophores described above covalently modifies the functional group through a well-characterized reaction. The general reaction mechanism for which is provided below:

IAF and IDANS: s-alkylation of thiols

Dansyl chloride:

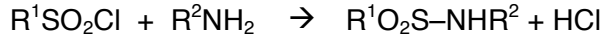

FITC

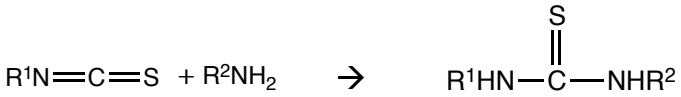

For convenience, a summary of the data from above is presented in a table below:

| **Fluorophore** | **Selectivity** | **$\lambda_{excitation}$** | **$\lambda_{emission}$** | **Solvent** | **Molar Absorptivity** | **Solvatochromism** |
|---|---|---|---|---|---|---|
| Dansyl chloride | Amine | 340 nm | 510 nm | Ethanol | 4700±400 $M^{-1}cm^{-1}$ | Positive |
| | | 341±3 nm | 491±4 nm | Chloroform | 4300 $M^{-1}cm^{-1}$ [ | |
| IDANS | Thiol | 336 nm | 520 nm | $H_2O$ | 5700±400 $M^{-1}cm^{-1}$ | Positive |
| | | 340 nm | 460 nm | Ethanol | | |
| | | 339 nm | 452 nm | Dioxane | | |
| FITC | Amine | 494±3 nm | 520±4 nm | 50mM potassium phosphate pH 9 | 78,000±7000 $M^{-1}cm^{-1}$ | Positive |
| IAF | Thiol | 492±3 nm | 515±4 nm | 50mM potassium phosphate pH 9 | 78,000±5000 $M^{-1}cm^{-1}$ | Positive |

**D. Previous progress in the laboratory**

Much progress has previously been made in the lab in studying protein oxidation and S-glutathiolation; this remains one of the primary research interests of the lab. Previous work has been directed towards the synthesis of fluorescently-labeled glutathione derivatives using FITC and dansyl chloride. Previous published work in the lab has described the synthesis and purification of fluorescein glutathione (F-GSH) as well as two derivatives of oxidized glutathione (GSSG), F-GSSG (F1) and F-GSSG-F (F2). [54] Additional published work in the lab has synthesized and purified dansyl glutathione (D-GSH) as well as D-GSSG (D1) and D-GSSG-D (D2) [55] We believe that the addition of the dansyl and fluorescein groups to glutathione does not affect the reactivity of the critical thiol; however, it is not known for sure since we are unable to compare with unlabeled GSH and GSSG.

Both D2 and F2 have been employed in the labeling of creatine kinase thiols with great success [55]. However, when the experiment was performed no direct comparison could be made between the different labeled samples due to the different fluorescent intensities of dansyl and fluorescein. Three primary labeling schemes were used to test the labeling of protein thiols, the first via thiol-disulfide exchange, where an oxidized protein is reacted with the labeled GSH; the second via the reduction of a mixed disulfide, where a labeled protein is reacted with a reducing agent, either dithiothreitoal (DTT) or tris((2-carboxyethyl)phosphine) (TCEP); and the third via the formation of a mixed disulfide, where a reduced protein is reacted with a labeled GSH in the presence of an oxidant. The first two label methods resulted in a protein containing a fluorescent label, while the second method resulted in the removal of the fluorescent label [55]. The fluorescence, as measured using an imaging camera, was the brightest for the third method, indicating that this method is the most efficient for the labeling of thiols with glutathione [55].

Previous work was primarily focused on using fluorescein-labeled glutathione, as its large fluorescence intensity allowed for easy labeling and purification. However, attempts to reduce F2 to F-GSH were unsuccessful, thought to be a result of steric hindrance due to the large size of the fluorescein molecule [54]. F1, however, was successfully reduced to F-GSH and GSH, and both D1 and D2 were also successfully reduced to D-GSH and GSH as well [55]. This limitation, in addition to both the pH and environmental effects on the fluorescein, resulted in a switch to dansyl-labeled glutathione in 2012.

To ensure that the addition of dansyl groups to glutathione does not affect its ability to label protein thiols, labeling experiments were performed using creatine kinase and GAPDH as reference proteins. Varying the percent composition of GSSG and D2 and observing the resulting fluorescent intensity revealed that an increase in the percent of GSSG over D2 resulted in a decrease in the fluorescent intensity, with the reverse effect observed as the percentage of D2 increased [55]. This indicates that there is no preference for GSSG over D2, meaning that the addition of dansyl groups does not affect the ability of glutathione to add to thiols [55]. This finding in particular enables dansyl-labeled glutathione to be used in the study of protein oxidation and repair.

While much work in the lab has been accomplished in this area, the results are largely qualitative. Fluorescent measurements were taken using an imaging camera with an excitation wavelength of 302 nm and the resulting image analyzed using quantitative software. This, however, provides no information regarding the fluorescence wavelength and different parameters that can contribute to the overall understanding of protein oxidation and repair. Therefore, the goal of this thesis is to develop a methodology to study protein S-glutathiolation using fluorescence spectroscopy.

# Materials and Methods

**Materials:**

Dansyl chloride, GSH, GSSG, IAF, papain, rabbit muscle creatine kinase (CK), and rabbit muscle glyceraldehyde-3-phosphate dehydrogenase (GAPDH) were obtained from Sigma (St. Louis, MO). Dithiolthreitol (DTT) and bovine serum albumin (BSA) were obtained from Fisher (Waltham, MA). Tris(2-carboxyethyl)phosphine (TCEP) and bicinchoninic acid (BCA) were obtained from Thermo Pierce (Rockford, Il). IDANS was obtained from Molecular Probes (Eugene, OR). FITC was obtained from Fluka (Seezle, Germany). All other chemicals were from Sigma or Fisher.

**Absorbance measurements:**

Absorbance measurements were performed using an Ocean Optics USB2000 spectrometer using the SpectraSuite software according to the directions from the manufacturer. Each measurement was performed in a quartz semimicro cuvette with a 1 cm path length and 1 mL sample volume. To ensure consistent measurements across different days, the following experimental parameters were used for each reading: 10,342 μs integration time and 5 scans to average. In addition, the absorbance of a 10 μM dansyl glycine (DG) standard, prepared from a 1 mM DG standard in 10 mM PB pH 7.4, was measured prior to each reading. Between readings, the cuvette was rinsed with DI and dried using a Kimwipe to minimize contamination of samples.

Beer's law was used to determine the concentration of the glutathione derivatives using the following molar absorptivity constants: FITC, $\varepsilon$=78,000 ± 7000 $M^{-1}cm^{-1}$ [42]; IAF, $\varepsilon$=78,000 ± 5000 $M^{-1}cm^{-1}$ [43]; IDANS, $\varepsilon$=5700 ± 400 $M^{-1}cm^{-1}$ [48], and dansyl chloride, $\varepsilon$=4300 $M^{-1}cm^{-1}$ [56].

**Fluorescence measurements:**

The fluorescence measurements were performed on a PerkinElmer LS 55 spectrofluorimeter with Fl WinLab software. The experimental parameters were varied depending on the molecule being studied and are provided below. Each measurement was performed in a quartz semimicro fluorimeter cell with a 10 mm pathlength and a 1 mL sample volume. To prevent any contamination between samples, the cuvette was rinsed with DI, dried with a Kimwipe, and rinsed with 1 mL of sample between measurements.

| **Dansyl chloride** | |
|---|---|
| Excitation λ: | 325 nm |
| Range: | 450-600 nm |
| Bandpass | 15 nm |
| Scan speed | 100 nm/min |

| **Dansyl acid** | |
|---|---|
| Excitation λ: | 310 nm |
| Range: | 400-600 nm |
| Bandpass | 15 nm |
| Scan speed | 100 nm/min |

| **Fluorescein** | |
|---|---|
| Excitation λ: | 325 nm |
| Range: | 480-600 nm |
| Bandpass | 15 nm |
| Scan speed | 100 nm/min |

| **GS–DANS** | |
|---|---|
| Excitation λ: | 337 nm |
| Range: | 450-600 nm |
| Bandpass | 15 nm |
| Scan speed | 100 nm/min |

| **BSA–DANS: native and EtOH-precipitated** | |
|---|---|
| Excitation λ: | 331 nm |
| Range: | 400-550 nm |
| Bandpass | 15 nm |
| Scan speed | 100 nm/min |

| SDS–PAGE purified BSA-DANS and SDS | |
|---|---|
| Excitation λ: | 300 nm |
| Range: | 325 nm |
| Bandpass | 15 nm |
| Scan speed | 100 nm/min |

| Papain–DANS: native and EtOH-precipitated | |
|---|---|
| Excitation λ: | 342 nm |
| Range: | 375-600 nm |
| Bandpass | 15 nm |
| Scan speed | 100 nm/min |

| Dansyl-labeled proteins | |
|---|---|
| Excitation λ: | 325 nm |
| Range: | 375-600 nm |
| Bandpass | 15 nm |
| Scan speed | 100 nm/min |

Similar to absorbance measurements, the fluorescence a 5 μM DG standard in 10 mM PB pH 7.4 was measured to ensure consistent readings across days.

**Camera fluorescence**

Fluorescence was also measured using a ChemiDoc XRS Imaging System. Measurements were performed in a 96 well black plate with a 200 μL sample volume. Imaging was performed using the Image Lab software with preset protocols: Ethidium bromide for dansyl-containing solutions and fluorescein for fluorescein-containing solutions. The fluorescence intensity was determined by integrating the volume of the resulting image.

**BCA assay**

To determine the protein concentration within a given sample, the BCA assay was performed with 1 mg/mL BSA standards according to the manufacturer's directions. The protein concentration in a given sample was determined from the absorbance at 562 nm using a BSA standard curve.

**D1 and D2 preparation:**

D1 and D2 were prepared from previously prepared and dried samples. The samples were resuspended in 10mM PB pH 7.4 and incubated at 37°C to ensure complete resuspension before use.

**DG preparation:**

A 20mM DG solution was prepared by adding 3.0 mg of DG to 487 uL of dimethylformamide (DMF). This standard solution was diluted to the appropriate concentration used for the absorbance and fluorescence measurements.

**D-GSH preparation**

To prepare D-GSH, a previously purified D2 sample was resuspended in 200 μL $H_2O$ followed by 300 μL of 0.1M Tris-HCl pH 7.4. After determining the D2 concentration, solid TCEP was added to achieve 5x the concentration of D2. The resulting D2+TCEP reaction was incubated at 37 °C for 30 minutes, or until D2 was sufficiently reduced as determined by thin-layer chromatography (TLC) with an 80:20:1 acetonitrile (AcCN): water ($H_2O$): acetic acid (HAc) running solution.

Once sufficiently reduced, the D2+TCEP reaction mixture was purified on a C8 column, with the purification procedure as follows. After loading the D2/TCEP solution, the column was washed with $H_2O$, 20% methanol (MeOH), and 100% MeOH washes containing 0.1% HAc. Column fractions were visualized using a hand-held UV light and tested for the presence of TCEP and free thiols by mixing an aliquot with the BCA reagent, which in the presence of TCEP and thiols, instantly turns brown and purple, respectively. The resulting fractions were then run on a TLC plate and visualized using UV light and ninhydrin to determine fraction composition.

D-GSH was predominantly found in the first 1mL 100% methanol wash, which was then aliquoted and dried in the SpeedVac overnight. Prior to use, the D-GSH pellet was resuspended in 10 mM PB pH 7.4.

**Dansyl acid preparation**

Dansyl acid was prepared from a solution of dansyl chloride (11.1 mM) in acetone. To this, 1 mL of 0.1 M sodium hydroxide (NaOH) was added and the solution was placed on ice for 1 hour with intermittent vortexing. After one hour, 1/100 of the total solution volume (20 µL) of HAc was added to neutralize the NaOH. Dansyl acid was purified from the reaction mixture by C8 column chromatography with $H_2O$ and MeOH washes containing 0.1% HAc and the column fractions visualized under UV light. As the MeOH washes exhibited the greatest fluorescence, they were dried under vacuum. Prior to use, the dansyl acid pellets were resuspended in 10 mM PB pH 7.4.

**F1 and F2 preparation**

F1 and F2 were prepared from a modified protocol from [54] with the following reagents: 50 mM FITC in DMF and 10 mM GSSG in 0.1 M ammonium bicarbonate. FITC (6.5 mM) was reacted with 6.5 or 7.5 mM GSSG (13 or 15 mM $RNH_2$) in 0.1 M ammonium bicarbonate buffer. The reactions were run at room temperature with stirring and periodically checked for product formation by TLC. Completed reactions were stored at 4 °C prior to purification.

The FITC/GSSG reaction (1 mL) was loaded on to a C8 column. After equilibrating, the load eluent was collected and labeled as fraction 1. The column was washed with 2x 500 µL $H_2O$ washes and labeled as fractions 2A and 2B. An additional 1 mL $H_2O$ wash was performed and labeled as fraction 3. Two, 1 mL MeOH washes were then performed and labeled fractions 4 and 5, respectively. The fraction composition was determined by TLC, where F1 and GSSG were

detected in fraction 2A and F2 detected in fraction 4. MeOH was removed from F2 under vacuum. Prior to analysis, the F2 pellet was resuspended in 150 µL of 10 mM PB pH 7.4.

**F-GSH preparation**

F-GSH was prepared from F1. Excess TCEP was added to F1 and the reaction was incubated at room temperature in the dark. No purification was performed on the F1/TCEP reaction prior to use.

**GS-AF preparation**

GS-AF was prepared using 10 mM IAF in DMF and 20 mM GSH in 10 mM PB pH 7.4. Three GSH/IAF reactions were prepared: 2:1, 4:1, and 6:1 GSH:IAF. Each contained 20 µL of IAF and 20, 40, and 60 µL of GSH for the 2:1, 4:1, and 6:1 reactions, respectively. Reaction progress was monitored by TLC with an IAF reference.

The GSH/IAF mixtures were pooled, the total volume brought to 1 mL with 10 mM PB pH 7.4, and purified on a C8 column with 3x1 mL $H_2O$ washes and 10%, 20%, 30%, 50%, and 100% MeOH washes. Column fractions were analyzed by TLC. GS-AF was detected in the $H_2O$ and the 30% MeOH washes. The 30% MeOH wash was left uncovered at room temperature to evaporate the MeOH.

**GS-DANS preparation**

GS-DANS was prepared from a 4:1 GSH:IDANS reaction mixture containing 80 µL of 20 mM GSH in 10 mM PB pH 7.4 and 40 µL of 10 mM IDANS in DMF. The GSH/IDANS mixture was incubated at room temperature for an hour with product formation periodically examined by TLC with an IDANS reference. The completed reaction was stored at 4 °C prior to purification.

The GSH/IDANS mixture was brought to a volume of 1 mL with 10 mM PB pH 7.4 before purifying by C8 chromotography. After loading the reaction and letting it equilibrate, the column was washed with DI, 10%, 20%, 50%, and 100% MeOH washes containing 1 µL/mL HAc. The fractions were visualized with UV light and fraction composition monitored by TLC with an IDANS reference, where it was shown that GS-DANS elutes entirely in the first $H_2O$ wash.

**BSA-DANS preparation**

BSA-DANS was prepared using the following reagents: 500 µL of 2 mg/mL BSA in 10 mM PB pH 7.4, 40 µL of 50 mM IDANS in DMF, and 1 µL of 100 mM TCEP in $H_2O$. The reaction proceeded at room temperature for 30 minutes with intermittent vortexing. BSA-DANS was separated from excess IDANS on a desalting column using the minimal dilution protocol from the manufacturer (Bio-rad), where the column was first equilibrated with 20 mL of 10 mM PB pH 7.4. After equilibrating, the sample volume was then added to the column and allowed to flow through. Once the sample was loaded onto the column, a total of (3 mL - sample volume) of buffer was added to the column and allowed to flow through. To elute the bound BSA-DANS, 8 mL of 10 mM PB pH 7.4 was added and 8 x 1 mL fractions were collected. The column was visualized under UV light to determine whether there was any remaining bound fluorescent material. In a departure from the manufacturer's directions, 2 additional 1 mL fractions were collected. All 10 fractions were then visualized under UV light and the protein concentration determined by BCA assay, which revealed that BSA-DANS was predominantly found in fractions 8,9, and 10, with fraction 9 having the highest amount of protein.

**Papain-DANS preparation**

Papain-DANS was prepared using a modified protocol from [57]. Papain (98.3 μM) was prepared in 500 μL of 10 mM PB pH 7.4. To this, 25 μL of 10 mM IDANS in DMF and 1 μL of 100 mM TCEP in $H_2O$ were added. The papain/IDANS mixture was incubated at 37 °C for 1 hour before purification on a desalting column with the minimal dilution protocol previously described. The protein content in each fraction was measured using the BCA assay, where papain-DANS was detected in fractions 3, 4, and 5.

**D-BSA preparation**

D-BSA was prepared using a procedure adapted from [58] with the following modifications: 0.1 M sodium bicarbonate buffer was used to dissolve the 5 mg/mL BSA instead of 0.2 M, and 200 μL of 50 mM dansyl chloride in acetone was used instead of 500 μL of 5 mM dansyl chloride. The reaction was incubated at room temperature for 1 hour with intermittent vortexing until the observed yellow color disappeared. Purification was performed using a variant of the minimal dilution protocol from Bio-rad. A 1.5 mL sample volume of D-BSA was loaded on the column. To that 1.5 mL of 10 mM PB pH 7.4 was added and allowed to flow through. D-BSA was collected in 1.5 x the sample volume (2.25 mL) of buffer.

**D-papain preparation**

D-papain was prepared using the protocol established by [58]. 5 mg papain was added to 500 μL of 0.2 M sodium bicarbonate, to that 500 μL of 5 mM dansyl chloride in acetone was added. After 1 hour at 37 °C, the labeled papain was purified by desalting with the minimal dilution protocol. The protein content was measured using the BCA assay, where it was determined that D-papain elutes in fractions 5 and 6.

**EtOH precipitation**

To precipitate a protein, 4 volumes of 100% ethanol (EtOH) was added to a protein sample, resulting in an 80% EtOH solution. This solution was then placed in the -20 °C freezer until a visible pellet had formed. Once a pellet had formed, the following procedure was performed: first, the 80% EtOH solution containing the pellet was centrifuged at 13,000 rpm for 10 mins. Next, the resulting supernatant was discarded and the pellet was washed with 500 µL of a chilled 80% EtOH solution. This solution was then centrifuged at 13,000 rpm for 5 min. The supernatant was discarded, the pellet was washed with 250 µL of chilled 80% EtOH, and centrifuged at 13,000 rpm for 5 min. This step was repeated until the supernatant was no longer fluorescent, or the fluorescence intensity of the supernatant did not change between washes. The microcentrifuge tube containing the pellet was inverted on a Kimwipe for 10 min to allow any remaining EtOH to evaporate. The pellet was resuspended with minimal 6 M guanidine hydrochloride (guHCl) before adding 10 mM PB pH 7.4 to a final solution volume of 500 µL.

**SDS PAGE purification of BSA-DANS**

Sodium dodecyl sulfate polyacrylamide gel electrophoresis (SDS PAGE) was run on two samples of BSA-DANS, per standard operating procedures, with 2, 7.5% 1.5 mm separating gels. The gels were run at 90 V for the first 15 minutes, followed by 115 V for the remaining hour. The gels were visualized with UV light source to reveal the BSA-DANS bands. These bands were excised from the gel and placed in a test tube containing 1.3 mL of 10 mM Tris pH 8.8 to allow the protein to elute from the gel prior to use.

**SDS preparation**

To prepare a 10% sodium dodecyl sulfate (SDS) solution, 1 g of SDS was brought to 10 mL with $H_2O$ and incubated at 37 °C until the SDS was completely dissolved. When not in use, the SDS solution was kept in the incubator to ensure that it remained dissolved.

**Oxidative labeling of proteins**

To label proteins with D-GSH, a reaction mixture containing 1 μg/μL of protein, 0.5 mM D-GSH, and 2 mM $H_2O_2$ was prepared and reacted for 15 minutes. After 15 minutes, iodoacetamide (IAM) was added to stop the reaction and block any unreacted cysteines. The labeled proteins were precipitated in 80% EtOH and purified via centrifugation before use

# Results

## A. Glutathione derivatives:

### a. Fluorescein glutathione

For all of the measurements described below the following buffers were used: 10 mM PB pH 8.5, 10 mM Tris pH 8.1, and 10 mM Tris pH 8.8. These buffers were selected as to ensure that fluorescein was in the dianionic form. Due to the large fluorescence quantum yield of fluorescein, the fluorescence spectra of F1, F2, and F-GSH were measured across a concentration range of 25-150 nM when measured with the fluorimeter and 25-200 nM with the camera. The fluorescence of GS-AF; however, was measured across a concentration range of 9.6-96 μM with the fluorimeter and 9.6-192 μM with the camera. For all of the fluorescein-containing molecules described below, the fluorescence intensity was linear with $R^2$ values greater than 0.97.

**i. Spectroscopic data for F1 and F2**

Buffer composition had no effect on both the absorbance and fluorescence maxima. F1 and F2 had absorbance maxima at 493±2 nm and fluorescence maxima at 516-518 nm. The emission intensities ranged from 126-860 for F1 and 125-770 for F2.

**ii. Spectroscopic data for F-GSH and GS-AF**

GS-AF

GS-AF had an absorbance maximum at 493±3 nm and an emission maximum at 512-515nm. The emission intensities ranged from 67 to 715.

F-GSH

There was no difference between the results for F-GSH and those of F1 and F2. Emission intensities were in the range of 120 to 846.

**iii. Summary of fluorescein data:**

| Molecule | Absorption wavelength (nm) | Emission wavelength (nm) | Intensity range |
|---|---|---|---|
| F1 | 493 ± 2 | 516-518 | 126-860 |
| F2 | 493 ± 2 | 516-518 | 125-770 |
| F-GSH (w/ TCEP) | 493 ± 2 | 516-518 | 67-715 |
| GS-AF | 493 ± 3 | 512-515 | 120-846 |

**iv. Representative spectra**

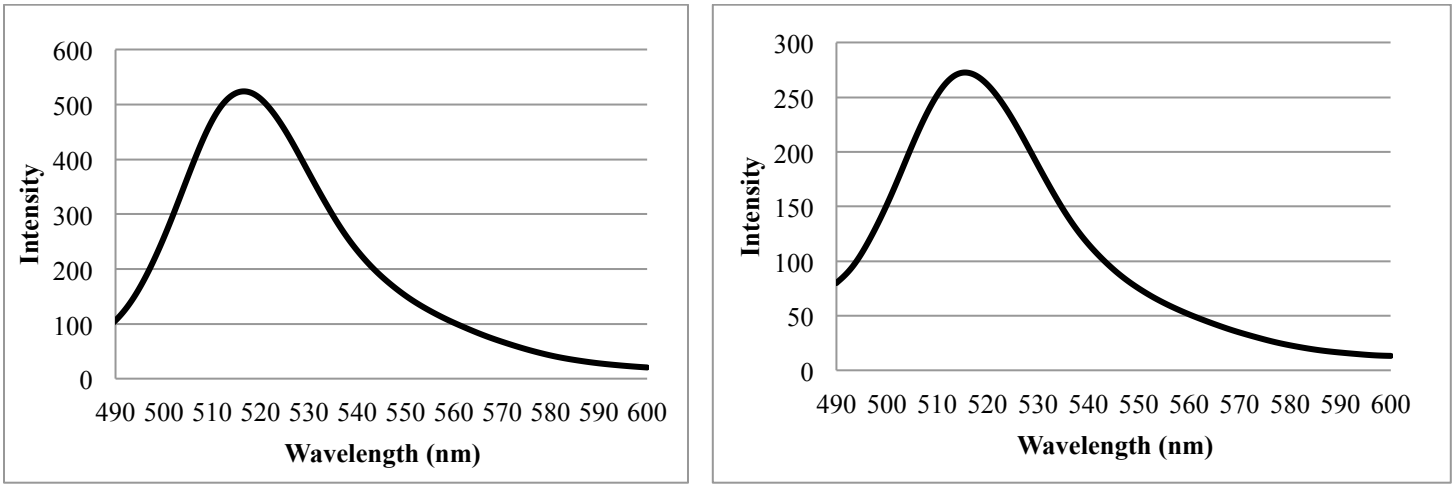


**Figure 9: Fluorescence emission spectra for 100 nM F2 (left) and 48 nM GS-AF (right) in 10 mM Tris pH 8.1, excitation at 325 nm**

**b. Dansyl glutathione**

**i. Spectroscopic results for DG, D1, and D2**

Absorption and fluorescence measurements were performed in 10 mM PB and 10 mM Tris with a pH range from 7.4 to 8.8. Buffer composition and pH were shown to have no effect on the absorbance and emission wavelengths for DG, D1, and D2. In addition, the fluorescence intensity of each molecule was demonstrated to be linear in the concentration range of 2.5-10 μM, with $R^2$ values greater than 0.96 when measured with both the camera and the fluorimeter.

DG

As DG served as the reference for all other measurements, its spectroscopic properties were first characterized. DG had an absorbance maximum at 327±2 nm and an emission maximum of 540±2 nm. Across the concentration range, the emission intensities for DG ranged from 117 to 390.

D1 and D2

Both D1 and D2 had absorbance maxima at 326±2nm and emission maxima at 538±2nm. Emission intensities ranged from 155 to 635 for D1 and 157 to 566 for D2.

**ii. Spectroscopic data for D-GSH and GS-DANS**

Absorption and fluorescence measurements were performed in 10 mM PB and 10 mM Tris in the pH range of 7.4 to 8.8. Buffer composition and pH had no effect on the absorption and fluorescence wavelengths. The fluorescence of both molecules was measured across a concentration range of 2.5 μM to 10.0 μM. Across this range, the fluorescence intensity was linear with $R^2$ values greater than 0.98 for D-GSH and 0.96 for GS-DANS when measured with both the camera and the fluorimeter.

D-GSH

To examine the effects of reducing agents on the spectroscopic properties of D-GSH, absorption and fluorescence measurements of D-GSH were performed with DTT and TCEP. The presence of DTT had no effect on the absorption and emission wavelengths of D-GSH, 326±2 nm and 536±3 nm, respectively. However, the presence of TCEP resulted in a decrease in the emission wavelength to 525-535 nm. Emission intensities for D-GSH without reducing agents ranged from 108-748.

GS-DANS

GS-DANS absorbed at a maximum wavelength of 337±2 nm and emitted at a maximum wavelength of 495±2 nm. Emission intensities ranged from 294-473 in 10 mM Tris pH 8.8.

**iii. Summary of dansyl data**

| Molecule | Absorption wavelength (nm) | Emission wavelength (nm) | Intensity range |
|---|---|---|---|
| DG | 327±2 | 540±2 | 117-390 |
| D1 | 326±2 | 538±2 | 155-635 |
| D2 | 326±2 | 538±2 | 157-566 |
| D-GSH | 326±2 | 536±3 | 108-748 |
| D-GSH + DTT | 327±2 | 537±3 | 138-518 |
| D-GSH + TCEP | 327±2 | 525-535 | 182-632 |
| GS-DANS | 337±2 | 495±2 | 294-473 |

**iv. Representative spectra….**

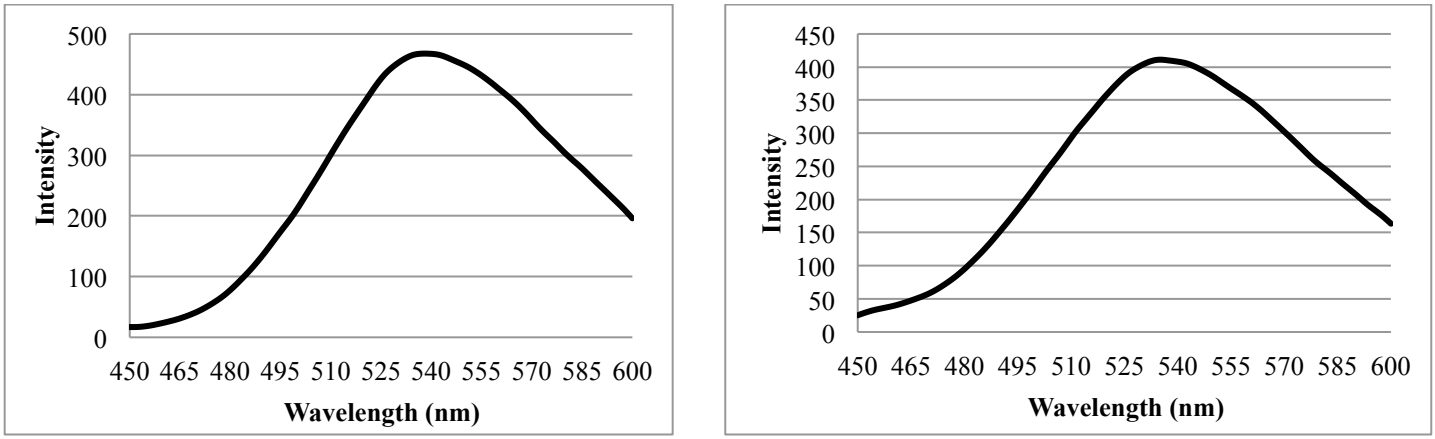


**Figure 10: Fluorescence emission spectra for 7.5 µM D1 (left) and 7.5 µM D-GSH (right) in 10 mM PB pH 7.4, excitation at 325 nm**

## B. $R_f$ Values for GS-AF and GS-DANS

The $R_f$ values for the molecules below were calculated using a 1μL sample size and run in a TLC plate with 80:20:1 AcCN:$H_2O$:HAc solvent mixture

GS-AF: $R_f$=0.35

GS-DANS: $R_f$=0.18

## C. Spectroscopic data for dansyl acid (dansyl sulfonic acid)

As dansyl acid is produced from unreacted dansyl chloride, its spectroscopic properties were characterized to ensure that no unreacted dansyl chloride was found in any of our samples. Absorbance measurements revealed that dansyl acid absorbs at a maximum wavelength of 310±2 nm in 10 mM PB pH 7.4. The fluorescence was measured in both 10 mM PB and 10 mM Tris in the pH range of 7.4 to 8.8. Buffer composition and pH had no effect on the fluorescence wavelength. Dansyl acid had an emission maximum at 501±2 nm. The fluorescence intensity of dansyl acid (84-628 μM) was linear across the range of 59-585 with $R^2$ values greater than 0.97.

## D. Summary of the proteins used:

Below is a table of the proteins used to examine S-glutathiolation

| Protein | Function | Molecular weight | Isoelectric point (pI) | Number of free cysteines |
|---|---|---|---|---|
| BSA [59] | Blood serum protein | 66,430 Da | 5.3 | 1 |
| Papain [60] | Cysteine protease | 23,406 Da | 8.75, 9.55 | 1 |
| Rabbit GAPDH [61,62] | Glycolytic enzyme | 36,000 Da (subunit) 144,000 Da (oligomer) | 8.5 | 4 |
| Rabbit CK [63,64] | ATP regeneration | 81,000 Da | muscle: 7.2 | 4 |

## E. BSA

### i. Spectroscopic data for D-BSA and BSA-DANS

D-BSA

Absorbance and fluorescence measurements for D-BSA were performed in 10 mM PB pH 7.4, 10 mM Tris pH 7.4, and 10 mM Tris pH 8.8. D-BSA had an absorbance maximum at 329±2 nm and an emission maximum at 513±2 nm. The fluorescence intensity of D-BSA (2.5-10 μM) ranged from 50-250 and was linear with $R^2$ values greater than 0.99.

BSA-DANS

Absorbance and fluorescence measurements for BSA-DANS were performed in the 10 mM PB pH 7.4, 10 mM Tris pH 7.4, and 10 mM PB 8.5. Independent of buffer composition and pH, BSA-DANS had an absorbance maximum at 331±2 nm and an emission maximum at 451±3 nm. The fluorescence intensity of BSA-DANS (81-810 nM) ranged from 100-954 and was linear with $R^2$ values greater than 0.95.

### ii. Spectroscopic data for denatured BSA-DANS

Two methods were used to denature BSA-DANS: SDS PAGE and EtOH precipitation. Absorbance measurements for the denatured BSA-DANS from both methods were performed in 10 mM PB pH 7.4. The absorbance spectra were negative-sloped lines beginning at 280nm and decreasing thereafter. There were no absorbance peaks within the region where dansyl typically absorbs, and thus no concentrations could accurately be determined. For this reason, the resulting concentration measurements used relative concentrations in μL/mL.

SDS PAGE purified BSA-DANS

Fluorescence measurements for the SDS PAGE purified BSA-DANS were performed in 10 mM PB pH 7.4. Emission spectra for the denatured BSA-DANS revealed two significant

peaks, one at 334±2 nm and the other at 463±3 nm, with the peak at 334±2 nm higher in intensity.

SDS

As the peak at 334±2 nm was significantly lower in wavelength than any previous sample, the fluorescence of SDS was measured to see if that was the cause. Addition of 1% SDS to BSA-DANS resulted in an emission peak at 335 nm. Additionally, the fluorescence of a 1% SDS solution in 10 mM PB pH 7.4 had an emission maximum at 334±2 nm

EtOH–precipitated BSA-DANS

Fluorescence measurements for the EtOH–precipitated BSA-DANS were performed in 10 mM PB pH 7.4. The EtOH-precipitated BSA-DANS emitted at a maximum wavelength of 463±2 nm. Addition of 6 M guHCl to native BSA-DANS decreased the emission maximum to 451 nm.

**iii. Summary of BSA data**

| Molecule | Absorption wavelength (nm) | Emission wavelength (nm) |
|---|---|---|
| D-BSA | 329 ± 2 | 513 ± 2 |
| BSA-DANS | 331 ± 2 | 451 ± 3 |
| EtOH–precipitated BSA-DANS | - | 463 ± 2 |
| BSA-DANS +6M guHCl | 330 | 451 |
| SDS PAGE denatured BSA-DANS | - | 463 ± 3 |
| BSA-DANS +1% SDS | 330 | 460 |
| SDS | - | 333 ± 2 |

### iv. Representative spectra

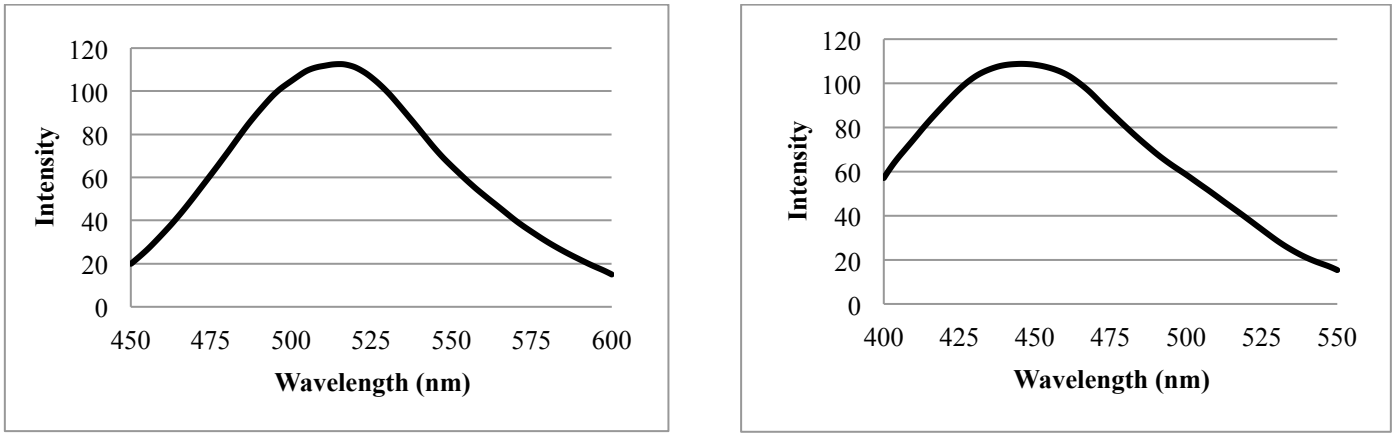


**Figure 11: Fluorescence emission spectra for 5 µM D-BSA (left) and 81 nM BSA-DANS (right) in 10 mM PB pH 7.4, excitation at 325 nm for D-BSA and 331 nm for BSA-DANS**

## F. Papain

### i. Spectroscopic data for D-papain and papain-DANS

Noisy absorbance spectra for D-papain and papain-DANS prevented accurate concentration determinations. Instead, concentrations were determined from the BCA assay with concentrations reported for papain rather than dansyl.

D-papain

Fluorescence measurements for D-papain were performed in 10 mM PB pH 7.4, 10 mM Tris pH 7.4, and 10 mM Tris pH 8.8. Buffer composition and pH had no effect on the fluorescence wavelength; D-Papain had an emission maximum at 505±3 nm. The fluorescence intensity of D-papain (43-270 nM) was linear across a range of 119 to 690 with $R^2$ values greater than 0.99 for all buffers expect 10 mM Tris pH 7.4, which had a lower $R^2$ value but still displayed linearity.

Papain-DANS

Fluorescence measurements for papain-DANS were performed in 10 mM PB pH 7.4 and 10 mM Tris pH 8.8. In all buffers, papain-DANS had an emission maximum at 497±3 nm. The fluorescence intensity of papain-DANS (55-390 nM) was linear across a range of 77-420 with $R^2$ values greater than 0.97.

EtOH-precipitated papain-DANS

Fluorescence measurements for EtOH-precipitated papain-DANS were performed in 10 mM PB pH 7.4. Measurements were performed on the same day as purification to prevent the degradation of the precipitated papain-DANS. EtOH-precipitated papain-DANS had an emission maximum at 481±3 nm. The fluorescence intensity was linear with an $R^2$ value greater than 0.99.

**ii. Summary of papain data**

| Molecule | Emission wavelength (nm) |
|---|---|
| D-papain | 505±3 |
| Papain-DANS | 497±3 |
| EtOH-precipitated papain-DANS | 481±3 |

**iii. Representative spectra**

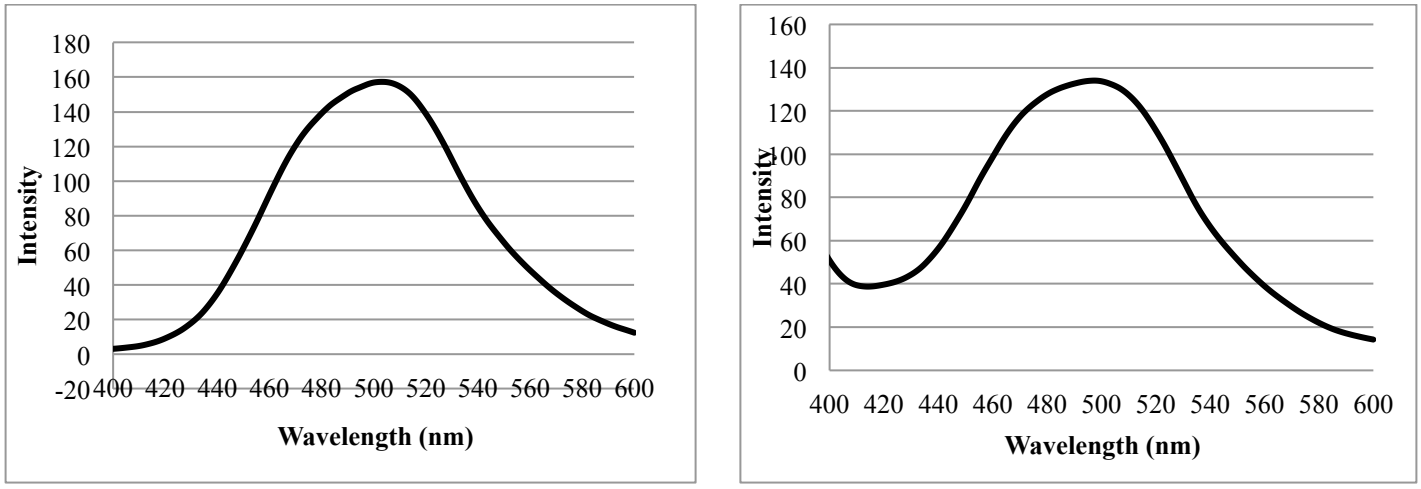


**Figure 12: Fluorescence emission spectra of 67 nM D-papain (left) and 57 nM papain-DANS (right) in 10 mM PB pH 7.4, excitation at 325 nm for D-papain and 331 nm for papain-DANS**

## G. Oxidative labeling with D-GSH

### i. Emission data

For each of the labeled proteins below, the fluorescence of 2 x 50 µL/mL samples was measured in 10 mM PB pH 7.4, 10 mM Tris pH 7.4, and 10 mM Tris pH 8.8. The buffer had no effect on the emission wavelength of the labeled protein.

BSA

Labeled BSA had an emission maximum at 505-507 nm and an average fluorescence intensity of 292 across all buffers.

Papain

Labeled papain had an emission maximum at 521 ± 2 nm and an average fluorescence intensity of 194 across all buffers.

CK

Labeled CK had an emission maximum at 507-510 nm and an average fluorescence intensity of 298 across all buffers.

GAPDH

Labeled GAPDH had an emission maximum at 510-512 nm and an average fluorescence intensity of 308 across all buffers.

### ii. Summary of data

| Protein | Emission wavelength (nm) | Average emission intensity |
|---|---|---|
| BSA | 505-507 | 292 |
| Papain | 519-523 | 194 |
| CK | 507-510 | 298 |
| GAPDH | 510-512 | 307 |

### iii. Representative spectra

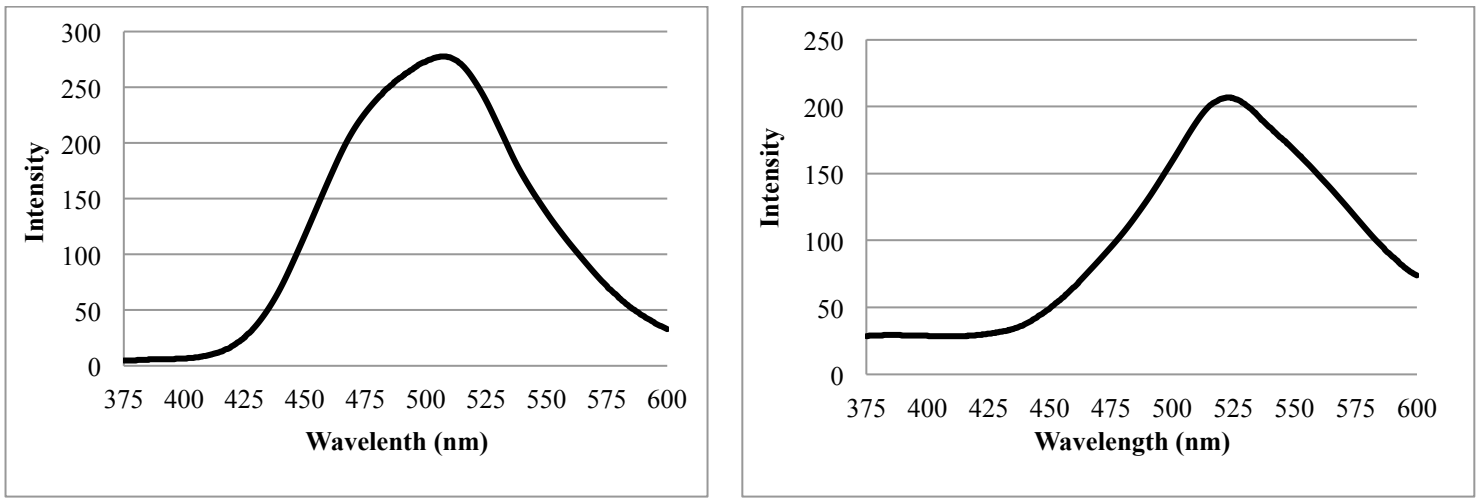


**Figure 13: Fluorescence emission spectra of 50 µL/mL labeled BSA (left) and papain (right) in 10 mM PB pH 7.4, excitation at 331 nm**

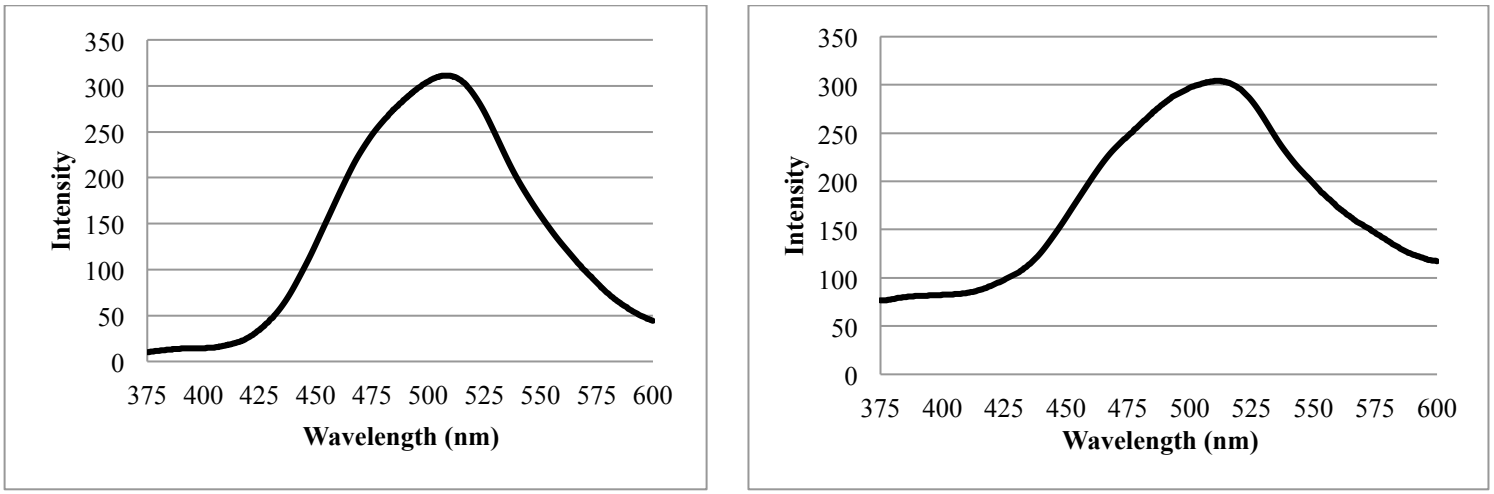


**Figure 14: Fluorescence emission spectra for 50 uL/mL labeled CK (left) and GAPDH (right) in 10 mM PB pH 7.4, excitation at 325 nm**

# Discussion:

### Dansyl vs. fluorescein

Dansyl and fluorescein have both been used in the lab to study S-glutathiolation; we have successfully synthesized and purified glutathione derivatives with both fluorophores and have successfully labeled proteins using both. However, both fluorophores have significant advantages and disadvantages. A significant advantage with fluorescein is that it has an intense absorbance, $\varepsilon$= 78,000 $M^{-1}cm^{-1}$ at 490 nm, and fluoresces with a high quantum yield, Q > 0.92, allowing for easy detection without irradiating with UV light. However, F2 cannot be reduced to F-GSH [55]. The advantages of dansyl are that both D1 and D2 are reduced with DTT and TCEP and undergo exchange with GSH [55]. However, dansyl has a weak absorbance, $\varepsilon$=4700 $M^{-1}cm^{-1}$ at 330 nm; it does not have a visible color unless highly concentrated; and the fluorescence of dansyl is dependent on the environmental polarity and the polarity of the protein that it is bonded to. Despite the apparent disadvantages of dansyl, the fact that F2 cannot be reduced makes dansyl the better fluorophore for our studies.

### Glutathione derivatives

Labeling of GSH and GSSG with dansyl and fluorescein had no effect on the absorption and emission wavelengths; D1, D2, and D-GSH all absorbed and emitted in the same region of the spectrum, 326 ± 3 nm and 536-540 nm, respectively. F1, F2, F-GSH, and GS-AF all absorbed and emitted in the same region of the spectrum, 493 ± 3nm and 512-518 nm, respectively. The only exception to this finding was GS-DANS, which absorbed at 337 ± 2 nm and emitted at 495 ± 2nm. However, the emission wavelength for IDANS is lower than dansyl chloride, 460 nm vs. 510 nm in EtOH, respectively. For each of the derivatives listed above, there was no fluorescence quenching; the fluorescence intensity was linear across the measured

concentration ranges. This removes any concentration limitations when using the glutathione derivatives.

**Dansyl acid**

The absorption and emission wavelengths for dansyl acid were significantly different than the wavelengths for dansyl glutathione; dansyl acid absorbs at 310 ± 2 nm and emits at 501 ± 2 nm, whereas D1 absorbs at 326 ± 2 nm and emits at 538 ± 2 nm. The differences in wavelength provide reasonable certainty that only the absorption and fluorescence of reacted dansyl were measured.

**EtOH precipitation vs. SDS PAGE**

Both EtOH precipitation and SDS PAGE are methods used to denature proteins into their primary structure. BSA-DANS was denatured by both methods with no effect on the emission wavelength; both the SDS PAGE purified BSA-DANS and EtOH-precipitated BSA-DANS had emission maxima at 463 ± 3 nm. This allows for both methods to be used to denature proteins. However, SDS contained an fluorescent impurity with an emission wavelength of 333 ± 2 nm. This finding was observed with both pure SDS obtained from C. J. Abelt, and the SDS used in the laboratory, which is optimized for the separation of proteins like tubulin. There was no observed fluorescence peak at 333 nm for the EtOH-precipitated BSA-DANS. For this reason, only EtOH precipitation was used to denature proteins.

**Comparison of Native BSA and papain**

Comparing the emission wavelengths of labeled BSA and papain against their GSH derivatives confirmed the positive solvatochromism of dansyl. The labeled proteins had a lower emission wavelength than their corresponding GSH derivatives, independent of the site of labeling. Intuitively these findings make sense, as the GSH derivatives were in a largely polar

environment surrounded by water and buffer molecules, whereas proteins are composed of both hydrophobic and hydrophilic residues that have a marked effect on the microenvironment surrounding an amino acid. In addition, a protein in its native state is folded in a three dimensional conformation that allows for different environments to exist within its structure, like a hydrophobic interior or a hydrophobic pocket.

There was a clear difference in the dansyl emission wavelengths for BSA and papain. This difference was greater when papain and BSA were labeled at cysteine; BSA-DANS had an emission wavelength of 451 ± 3 nm and papain-DANS had an emission wavelength of 497 ± 3 nm, a difference of over 50 nm. Labeling at amines also resulted in a difference in the emission wavelength, though it was not as great as the difference from cysteine labeling. D-papain had an emission wavelength of 505 ± 3 nm and D-BSA had an emission wavelength of 513 ± 2nm, a difference of only 8 nm. Labeling at cysteine provides more information in the study of S-glutathiolation as it provides information about the microenvironment surrounding a RSH.

Two factors can account for the differences in the emission wavelengths for BSA-DANS and papain-DANS. First, BSA is a largely hydrophobic protein whereas papain is comparatively hydrophilic. The positive solvatochromism of dansyl explains the lower emission wavelength of BSA-DANS relative to papain-DANS. In addition, BSA, which has a pI of 5.3, is negatively charged at physiological pH. Papain, which has pIs of 8.75 and 9.55, is positively charged at physiological pH. However, without data for more proteins labeled with IDANS, it is difficult to determine the effect of pI and charge on the dansyl emission wavelength.

In addition to the observed wavelength effects, there was a difference in the emission intensities between BSA and papain. BSA-DANS (81-810 nM) had emission intensities in the

range of 100-954, whereas papain-DANS (55-220 nM) had emission intensities in the range of 111-420.

**Effect of unfolding on BSA-DANS and papain-DANS**

Unfolding had an effect on the emission wavelength for BSA-DANS and papain-DANS. Native BSA-DANS had an emission wavelength of 451 ± 3 nm whereas unfolded BSA-DANS had an emission wavelength of 463 ± 2 nm. The increase in wavelength for BSA-DANS is explained by the fact that unfolding a protein exposes buried residues to the solvent, which is more polar than the folded protein. However, the same effect was not observed for papain-DANS; native papain-DANS had an emission wavelength of 497 ± 3 nm and unfolded papain-DANS had an emission wavelength of 481 ± 3 nm.

**Oxidative labeling of proteins with D-GSH**

There was an observable difference between the emission wavelengths for the proteins labeled with D-GSH. Labeled BSA had an emission wavelength of 505-507 nm, labeled papain had an emission wavelength of 519-523 nm, labeled CK had an emission wavelength of 507-510 nm, and labeled GAPDH had an emission wavelength of 510-512 nm. The differences in the emission wavelengths were not the result of the preparation; each protein was labeled and precipitated in the same way, including using the same amounts of guHCl to resuspend the protein pellets. Thus, any observed differences in the emission wavelengths are due to the protein itself. These differences may be correlated to the pI of the protein; where, as the pI of the protein increases the emission wavelength likewise increases. BSA, which has the lowest pI of 5.3, has the lowest emission wavelength, whereas papain, which has pIs of 8.75 and 9.55, emits at the highest wavelength. This trend is continued with GAPDH and CK; GAPDH, which has a pI of 8.5, emits at a higher wavelength than CK, which has a pI of 7.2. The difference in the emission

wavelengths between GAPDH and CK; however, is not as large as the difference between papain and BSA. We think that this is due to the fact that BSA and papain only have one cysteine, whereas GAPDH and CK have 4 cysteines; the emission wavelength for GAPDH and CK results from multiple sites of labeling, and thus multiple environments, whereas the emission wavelength for BSA and papain is the result from a single labeling site. Better understanding of the labeling procedure would help to clarify this issue.

**Conclusion and future directions**

The goal of this project was to develop a model of protein oxidation and repair using fluorescence spectroscopy. The results herein represent significant progress towards this goal. Labeling of BSA and papain with IDANS showed a difference in the cysteine residues between the proteins, a fact that was confirmed when both proteins were oxidatively labeled with D-GSH However, these results are not widely applicable as both BSA and papain have only one cysteine residue. To extend this model, GAPDH and CK were oxidatively labeled with D-GSH. Labeling of both GAPDH and CK showed a difference in the emission wavelength between the proteins; however, it was not clear which cysteines were oxidized. Despite this, there was a clear difference between the two proteins. Both GAPDH and CK undergo S-glutathionylation [65,66], and oxidation of both proteins is implicated in neuronal cell death [67,68]. Thus, this model has the potential to greatly increase the efforts in the lab to understand of protein oxidation and repair and how it relates neurodegeneration.

While this model has shown great potential, it needs refinement. Although there was a difference in the emission wavelength for the GAPDH and CK, it was unknown which cysteines were labeled with D-GSH. In addition, it would be useful to understand the effect of the concentration of D-GSH on labeling. Currently, this model has been used with proteins

containing up to 4 cysteines. This limits the applicability of the model in studying tubulin oxidation and repair, as tubulin has 20 cysteines. Extending the model to proteins with more cysteines would help to increase the applicability to tubulin. In addition, all proteins used in the experiments were purified proteins obtained from commercial sources. We are currently developing a model of protein oxidation using *Saccharomyces cerevisae* (baker's yeast) protein extracts. Using yeast instead of the porcine tubulin currently used in the laboratory would simplify characterization of tubulin oxidation; yeast has 3 tubulin gene products compared the multiple gene products of mammalian tubulin [69]. Overall, the work herein provides a promising direction for future research in the Landino laboratory.

# References


[1] F.S. Wouters, P.J. Verveer, P.I.H. Bastiaens, Imaging biochemistry inside cells, TRENDS in Cell Biology 11:5 (2001) 203-211

[2] B.N. Giepmans, S.R. Adams, M.H. Ellisman, R.Y. Tsien, The Fluorescent Toolbox for Assessing Protein Location and Function, Science 312 (2006) 217-224

[3] S. Duan, X. Guan, R. Lin, X. Liu, Y. Yan, R, Lin, T. Zhang, X. Chen, J. Huang, X. Sun, Q. Li, S. Fang, J. Xu, Z. Yao, H. Gu, Silibinin inhibits acetylcholinesterase activity and amyloid β peptide aggregation: a dual-target drug for the treatment of Alzheimer's disease, Neurobiology of Aging (2015) 1-16

[4] X. Liu, J. Little, Z. Yuan, Glycolytic metabolism influences global chromatin structure, Oncotarget 6:6 (2015) 4214-4225

[5] Y. Lai, Y. Chang, L. Hu, Y. Yang, A. Chao, Z. Du, J. Tanner, M. Chye, C. Qian, K. Ng, H. Li, H. Sun, Rapid labeling of intracellular His-tagged proteins in living cells, PNAS 112:10 (2015) 2948-2953

[6] B. Haines, J. Hughes, M. Corbett, M. Shaw, J. Innes, L. Patel, J. Gecz, J. Clayton-Smith, P. Thomas, Interchromosomal insertional translocation at Xq26.3 alters SOX3 expression in an individual with XX male sex reversal, Journal of Endocrinology & Metabolism (2015) doi: 10.121/jc.2014-4383

[7] F.G. Ortega, J.A. Lorente, J.L. Garcia Puche, M.P. Ruiz, R.M. Sanchez-Martin, D. de Miguel-Pérez, J.J. Diaz-Mochon, M.J. Serrano, miRNA in situ hybridization in

circulating tumor cells – MishCTC, Scientific Reports 5:9207 (2015) doi:10.1038/srep09207

[8] M. Zimmer, Green Fluorescent Protein (GFP): Applications, Structure, and Related Photophysical Behavior, Chem. Rev. 102 (2002) 759-781

[9] M. Ehrenberg, The green fluorescent protein: discovery, expression and development, Scientific Background on the Nobel Prize in Chemistry 2008

[10] D.S. Talaga, W. Leung Lau, H. Roder, J. Tang, Y. Jia, W.F. DeGrado. R.M. Hochstrasser, Dyanmics and folding of single two-stranded coiled-coil peptides studied by fluorescent energy transfer confocal microscopy, PNAS 97:24 (2000) 13201-13206

[11] B. Schuler, W.A. Eaton, Protein folding studied by single-molecule FRET, Current Opinion in Structural Biology 18 (2008) 16-26

[12] A.E. Albers, V.S. Okreglak, C.J. Chang, A FRET-Based Approach to Ratiometric Fluorescence Detection of Hydrogen Peroxide, J. Am. Chem. Soc. 128 (2006) 9640-9641

[13] D. Zhu, L. Xue, G. Li, Y. Che, H. Jiang, A turn-on fluorescent probe for detection of hydrogen sulfide in aqueous solution and living cells, Org. Chem Front. 1 (2014) 501-505

[14] J. Tao, P. Song, Y. Sato, S. Nishizawa, N. Teramae, A. Tong, Y. Xiang, A label-free and sensitive fluorescent method for the detection of uracil-DNA glycosylase activity, Chem. Commun. 51 (2015) 929-932

[15] C. Lei, Z. Wang, Z. Nie, H. Deng, H. Hu, Y. Huang, S. Yao, Resurfaced Fluorescent Protein as a Sensing Platform for Label-Free Detection of Copper(II) Ion and Acetycholinesterase Activity, Anal. Chem. 87 (2015) 1974-1980

[16] D. Baskíc, S. Popović, P. Ristić, N.N. Arsenijević, Analysis of cyclohexamide-induced apoptosis in human leukocytes: Fluorescence microscopy using annexin V/propidium iodide versus acridin orange/ethidium bromide, Cell Biology International 30 (2006) 924-932

[17] S. Burmakina, Y. Geng, Y. Chen, Q.R. Fan, Heterodimeric coiled-coil interactions of human $GABA_B$ receptor, PNAS 111:19 (2014) 6958-6963

[18] H. Yu, Extending the size limit of protein nuclear magnetic resonance, PNAS 96 (1999) 332-334

[19] G.S. Waldo, B.M. Standish, J. Berendzen, T.C. Terwilliger, Rapid protein-folding assay using green fluorescent protein, Nature Biotechnology 17 (1999) 691-695

[20] S. Chiantia, J. Ries, P. Schwille, Fluorescence correlation spectroscopy in membrane structure elucidation, Biochimica et Biophysica Acta 1788 (2009) 225-233

[21] F. Fernandes, A. Coutinho, M. Prieto, L.M.S. Loura, Electrostatically driven lipid-protein interaction: Answers from FRET, Biochimica et Biophysica Acta (2015) doi: 10.1016/j.bbamem.2015.02.023

[22] A.I. Tomescu, N.C. Robb, N. Hengrung, E. Fodor, A.N. Kapanidis, Single-molecule FRET reveals a corkscrew RNA structure for the polymerase-bound influenza virus promoter, PNAS (2014) E3335-E3342

[23] R.D. Johnson, D.G. Steel, A. Gafni, Structural evolution and membrane interactions of Alzheimer's amyloid-beta peptide oligomers: New knowledge from single-molecule fluorescence studies, Protein Science 23 (2014) 869-883

[24] K.J. Amann, T.D. Pollard, Direct real-time observation of actin filament branching mediated by Arp2/3 complex using total internal reflection fluorescence microscopy, PNAS 98:26 (2001) 15009-15013

[25] K. Truong, M. Ikura, The use of FRET imaging microscopy to detect protein-protein interactions and protein conformational changes in vivo, Current Opinion in Structural Biology 11 (2001) 573-578

[26] Y. Zhao, Q, Fang, A.D. Herbst, K.N. Berberian, W. Almers, M. Lindau, Rapid structural change in synaptosomal-associated protein 25 (SNAP25) precedes the fusion of single vesicles with the plasma membrane in live chromaffin cells, PNAS 110:35 (2013) 14249-14254

[27] H. Yamashita, Y. Yano, K. Kawano, K. Matsuzaki, Oligomerization-function relationship of EGFR on living cells detected by the coiled-coil labeling and FRET microscopy, Biochimica et Biophysica Acta 1848 (2015) 1359-1366

[28] P. Klatt, S. Lamas, Regulation of protein function by S-glutathiolation in response to oxidative and nitrosativestress, Eur. J. Biochem 267 (2000) 4928-4944

[29] I. Dalle-Donne, R. Rossi, D. Giustarini, R. Colombo, A. Milzani, S-glutathionylation in protein redox regulation, Free Radical Biology & Medicine 43 (2007) 883-898

[30] B.G. Hill, A. Bhatnagar, Protein S-glutathiolation: Redox-sensitive regulation of protein function, J. Mol. Cell. Cardiol. 52:3 (2012) 559-567

[31] D. Giustarini, R. Rossi, A. Milzani, R. Colombo, I. Dalle-Donne, S-Glutathionylation: from redox regulation of protein functions to human diseases, J. Cell. Mol. Med. 8:2 (2004) 201-212

[32] L.M. Landino, K.L Moynihan, J.V. Todd, K.L Kenett, Modulation of the redox state of tubulin by the glutathione/glutaredoxin reductase system, Biochemical and Biophysical Research Communications 314 (2004) 555-560

[33] R.F. Ludueña, A Hypothesis on the Origin and Evolution of Tubulin, International Review of Cell and Molecular Biology 302 (2013) 41-185

[34] L.M. Landino, R. Hasan, A. McGaw, S. Cooley, A.W. Smith, K. Masselam, G. Kim, Peroxynitrite Oxidation of Tubulin Sulfhydryls Inhibits Microtubule Polymerization, Archives of Biochemistry and Biophysics 398:2 (2002) 213-220

[35] L.M. Landino, M.T. Koumas, C.E. Mason, J.A. Alston, Modification of Tubulin Csteins by Nitric Oxide and Nitroxyl Donors Alters Tubulin Polymerization Activity, Chem. Res. Toxicol. 20 (2007) 1693-1700

[36] L.M. Landino, T.D. Hagedorn, S.B. Kim, K.M. Hogan, Inhibiton of tubulin polymerization by hypochlorous acid and chloramines, Free Radical Biology and Medicine, 50 (2011) 1000-1008

[37] C. Lind, R. Gerdes, Y. Hamnell, I. Schuppe-Koistinen, H. Brockenhuus von Löwenhielm, A. Holmgren, I.A. Cotgreave, Identification of S-glutathionylated cellular proteins during oxidative stress and constitutive metabolism by affinity purification and proteomic analysis, Archives of Biochemistry and Biophysics 406 (2002) 229-240

[38] L.M. Landino, S.H. Robinson, T.E. Skreslet, D.M. Carbal, Redox modulation of tau and microtubule-associated protein-2 by the glutaredoxin reductase system, Biochemical and Biophysical Research Communications 323 (2004) 112-117

[39] D. Magde, R. Wong, P.G. Seybold, Fluorescence Quantum Yields and Their Relation to Lifetimes of Rhodamine 6G and Fluorescein in Nine Solvents: Improved Absolute Standards for Quantum Yields, Photochem. and Photobio. 75:4 (2002) 327-334

[40] R. Sjöback, J. Nygren, M. Kubista, Absorption and fluorescence properties of fluorescein, Spectrochemica Acta Part A 51 (1995) L7-L21

[41] D. Marguiles, G. Melman, A. Shanzer, Fluorescein as a model molecular calculator with reset capability, Nature Materials 4 (2005) 768-711

[42] Molecular Probes, FITC Certificate of Analysis, Invitrogen Corporation

[43] Molecular Probes, IAF Certificate of Analysis, Invitrogen Corporation

[44] T. Yogo, Y. Urano, A. Mizushima, H. Sunahara, T. Inoue, K. Hirose, M. Lino, K. Kikuchi, T. Nagano, Selective photoinactivation of protein function through environment-sensitive switching of single oxygen generation by photosensitize, PNAS 105:1 (2008) 28-32

[45] F. Naderi, A. Farajtabar, F. Gharib, Solvatochromic and preferential solvation of fluorescein in some water-alcoholic mixed solvents, Journal of Molecular Liquids 190 (2014) 126-132

[46] V.A Spivak, V.V. Scherbukhin, V.M. Orlov, JA.M Varshavsky, Quantitative Ultramicroanlysis of Amino Acids in the Form of their DNS-Derivatives, Analytical Biochemistry 39 (1971) 271- 281

[47] R.R. Hill, C.W. Richenburg, D.R. Roberts, Relative fluorescence yields of dansyl amino acids: a sensitive probe for structures in solution, Journal of Photochemistry and Photobiology A: Chemistry 97 (1996) 109-112

[48] Molecular probes, Dansyl chloride Certificate of Analysis, Invitrogen Corporation

[49] E.N. Hudson, G. Weber, Synthesis and Characterization of Two Fluorescent Sulfhydryl Reagents, Biochemistry 12:21 (1973) 4154-4161

[50] Molecular Probes, 1,5-IAEDANS Certificate of Analysis, Invitrogen Corporation

[51] R.F. Chen, Fluorescence of Dansyl Amino Acids in Organic Solvents and Protein Solutions, Archives of Biochemistry and Biophysics 120 (1967) 609-620

[52] R.F. Chen, Fluorescence lifetime reference standards for the range 0.189 to 115 nanoseconds, Anal. Biochem. 57:2 (1974) 593-604

[53] P. Hammarström, R. Owenius, L-G. Mårtensson, U. Carlsson, M. Lindgren, High-Resolution Probing of Local Conformational Changes in Proteins by the Use of Multiple Labeling: Unfolding and Self-Assembly of Human Carbonic Anhydrase II Monitored by Spin, Fluorescent, and Chemical Reactivity Probes, Biophysical Journal 80 (2001) 2867-2885

[54] L.M. Landino, C.M. Brown, C.A. Edson, L.J. Gilbert, N. Grega-Larson, AJ Wirth, K.C. Lane, Fluorescein-labeled glutathione to study protein S-glutathionylation, Analytical Biochemistry 402 (2010) 102-104

[55] L.M. Landino, S.E Hartzell, O.J. Blazek, T.K. Lain, Dansyl- and fluorescein-modified glutathione to study protein thiol reactivity and S-glutathionylation, Society for Free Radical Biology and Medicine conference, San Diego, CA November 15-18, 2012

[56] R.F. Chen, Determination of Extinction Coefficient and Number of Bound Residues with Radioactive Dansyl Chloride, Analytical Biochemistry 25 (1968) 412-416

[57] P. Lindahl, E. Raub-Segall, S.T. Olson, I. Björk, Papain labeled with fluorescent thiol-specific reagents as a probe for characterization of interactions between cysteine protesases and their inhibitors by competitive titrations, Biochemical Journal 276 (1991) 387-394

[58] W.R. Gray, Dansyl Chloride Procedure, Methods in Enzymology 11 (1967) 139-151

[59] Sigma-Aldrich Corporation, Albumin from Bovine Serum Product Information

[60] Sigma-Aldrich Corporation, Papain from papaya latex Product Information

[61] Worthington Biochemical Corporation, Glyceraldehyde-3-Phosphate Dehydrogenase, Worthington Enzyme Manual

[62] L.M. Landino, T.D. Hagedorn, K.L. Kennett, Evidence for Thiol/Disulfide Exchange Reactions Between Tubulin and Glyceraldehyde-3-Phosphate Dehydrogenase, Cytoskeleton 71 (2014) 707-718

[63] Worthington Biochemical Corporation, Creatine Kinase, Worthington Enzyme Manual

[64] S.H. Grossman, Electrophoresis of Creatine Kinases: A Laboratory Experiment in Isozymes, Biochemical Education 10:1 (1982) 8-10

[65] S. Reddy, A.D. Jones, C.E. Cross, P.S-Y. Wong, A. van der Vliet, Inactivation of creatine kinase by S-glutathionylation of the active-site cysteine residue, Biochem. J. 347 (2000) 821-827

[66] S. Mohr. H. Hallak, A. de Boitte, E.G. Lapetina, B. Brüne, Nitric Oxide-induced S-Glutathionylation and Inactivation of Glyceraldehyde-3-phosphate Dehydrogenase, The Journal of Biological Chemistry 274:14 (1900) 9427-9430

[67] T.S. Bürklen, U. Schlattner, R. Homayouni, K. Gough, M. Rak, A. Szeghalmi, T. Wallimann, The Creatine Kinase/Creatine Connection to Alzheimer's Disease: CK Inactivation, APP-CK Complexes, and Focal Creatine Desposits, Journal of Biomedicine and Biotechnology, 2006 (2006) 1-11

[68] H. Nakajima, W. Amano, A. Fujita, A. Fukuhara, Y.-T. Azuma, F. Hata, T. Inui, T. Takeuchi, The Active Site Cysteine of the Proapoptotic Protein Glyceraldehyde-3-phosphate Dehydrogenase Is Essential in Oxidative Stress-induced Aggregation and Cell Death, J. Biol. Chem 282 (2007) 26562-26574

[69] G. Barnes, K. A. Louie, D. Bolstein, Yeast proteins associated with microtubules in vitro and in vivo, Mol. Biol. Cell. 3 (1992) 29-47

# Appendix: Supplementary Figures

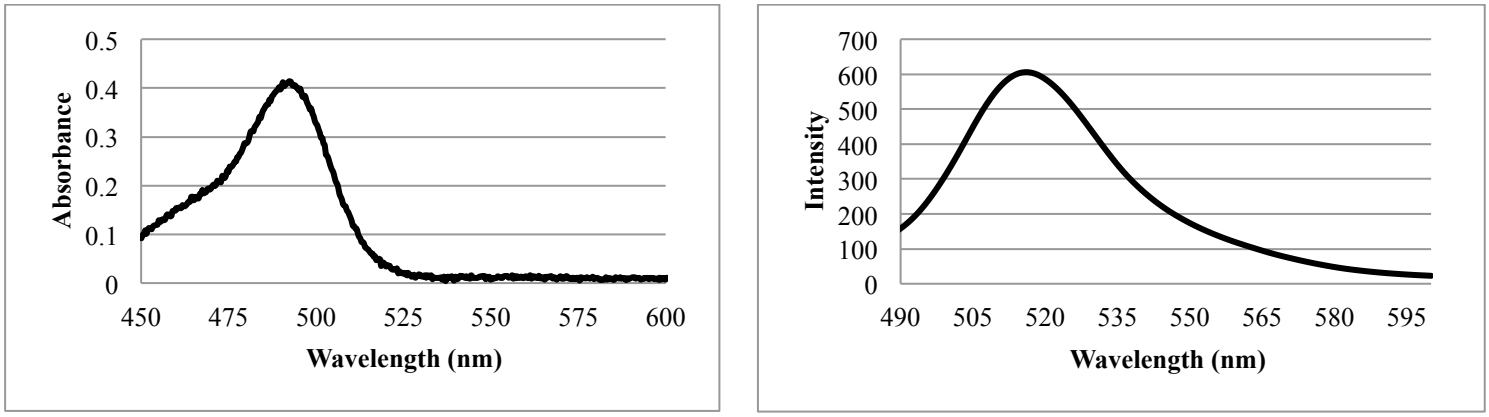


**Figure 15: Absorbance spectrum of 2.68 mM F1 (left) and emission spectrum of 100 nM F1 (right) in 10 mM Tris pH 8.8**

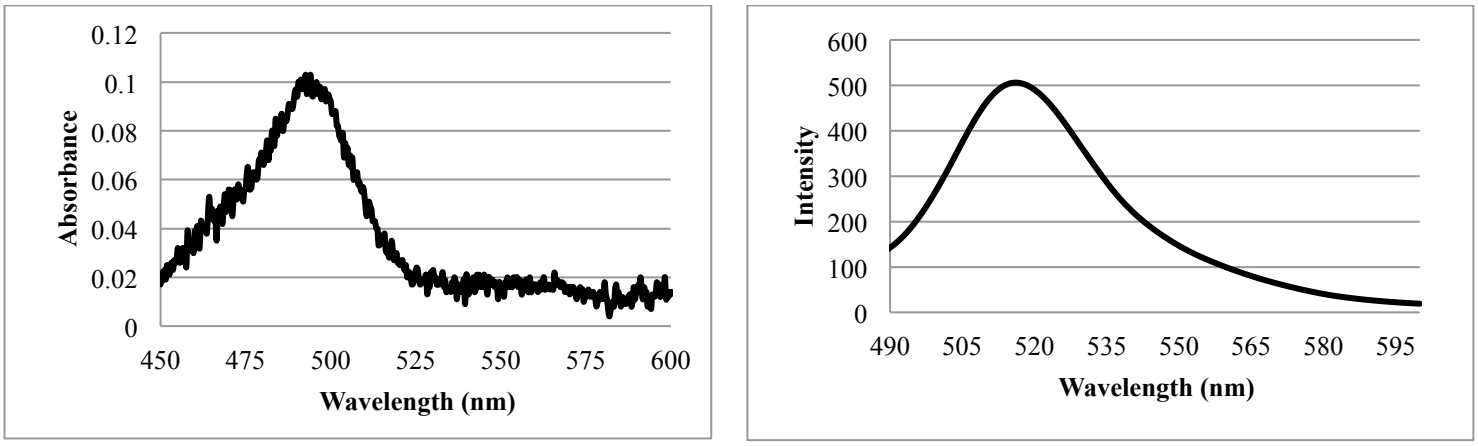


**Figure 16: Absorbance spectrum of 0.67 mM F2 (left) and emission spectrum of 100 nM F2 (right) in 10 mM Tris pH 8.8**

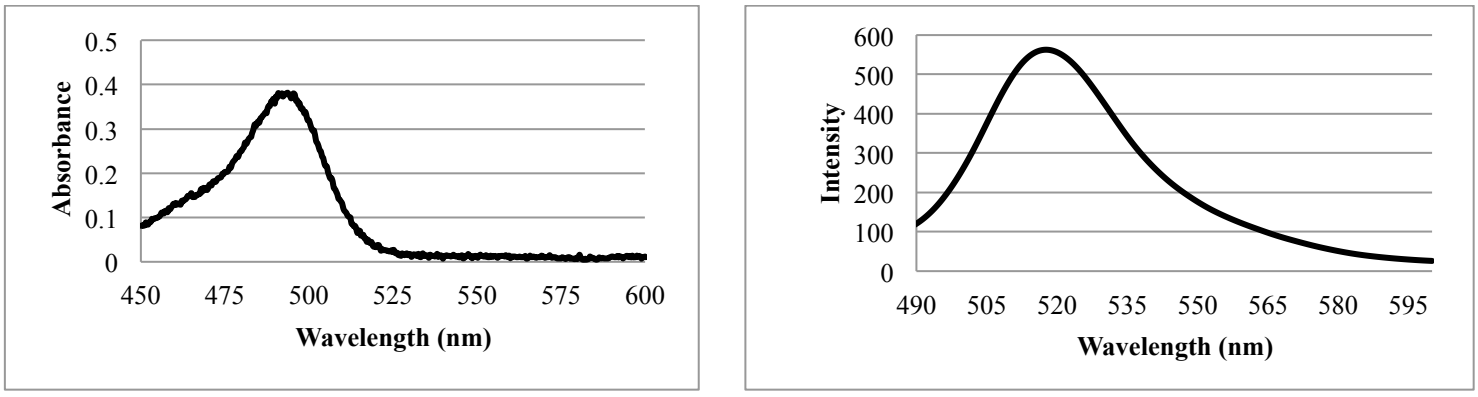


**Figure 17: Absorbance spectrum of 2.48 mM F-GSH (left) and emission spectrum of 100 nM F-GSH (right) in 10 mM Tris pH 8.8**

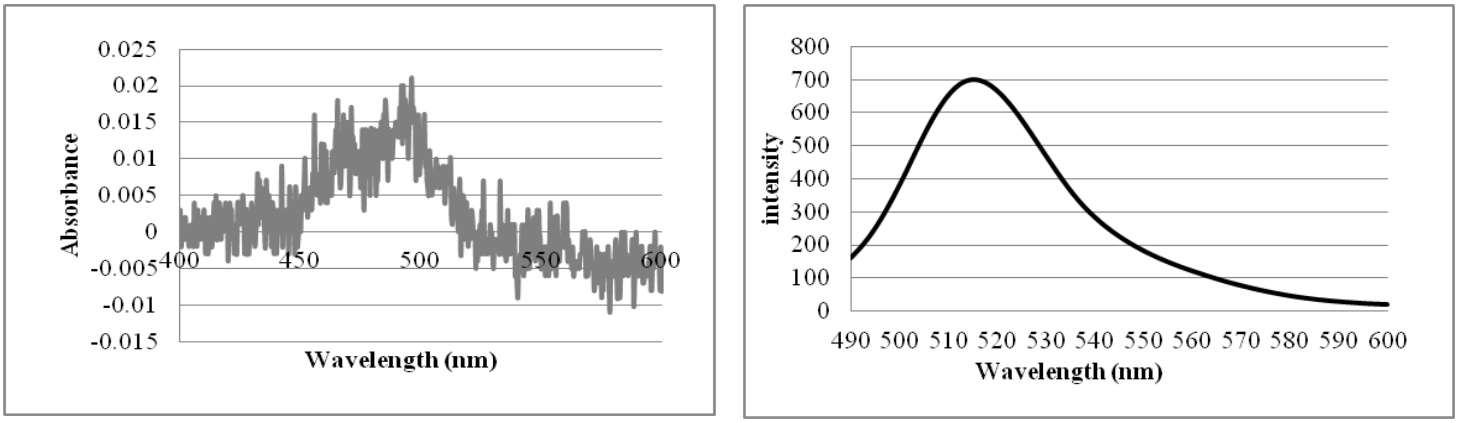


**Figure 18: Absorbance spectrum of 0.14 mM GS-AF (left) and emission spectrum of 136 µM GS-AF (right) in 10 mM Tris pH 8.8**

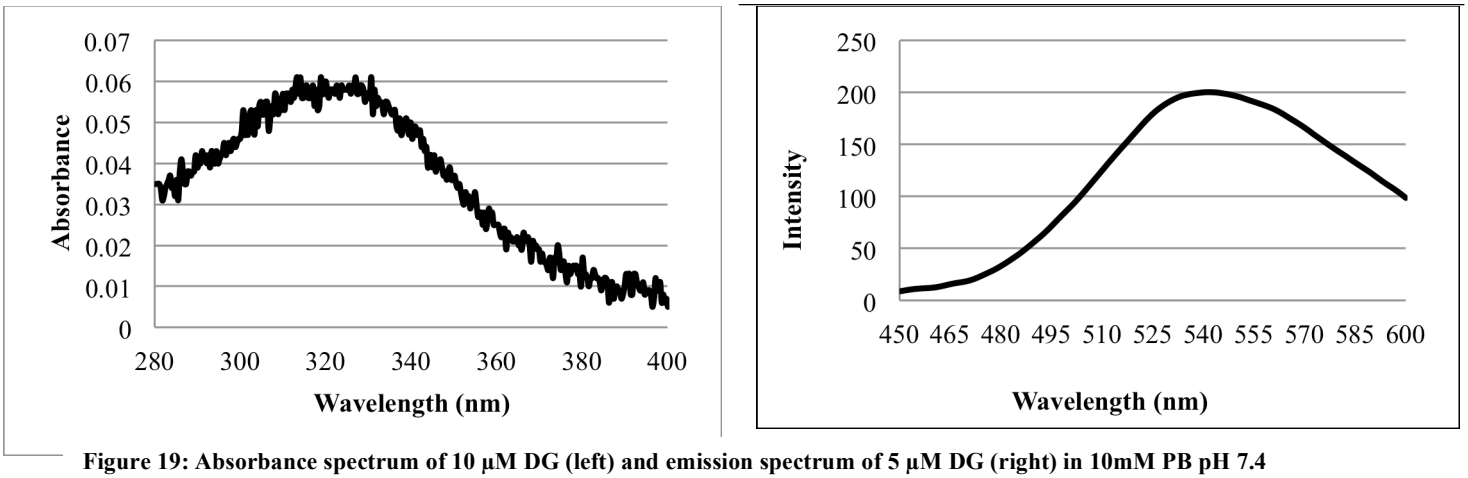


**Figure 19: Absorbance spectrum of 10 µM DG (left) and emission spectrum of 5 µM DG (right) in 10mM PB pH 7.4**

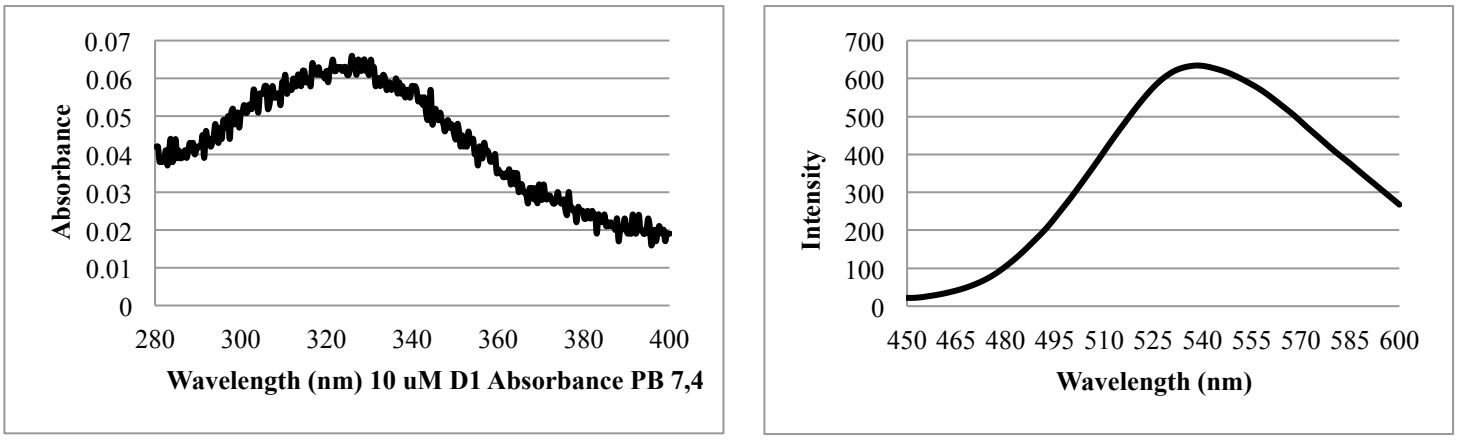


**Figure 20: Absorbance (left) and emission (right) spectra of 10 µM D1 in 10 mM PB pH 7.4**

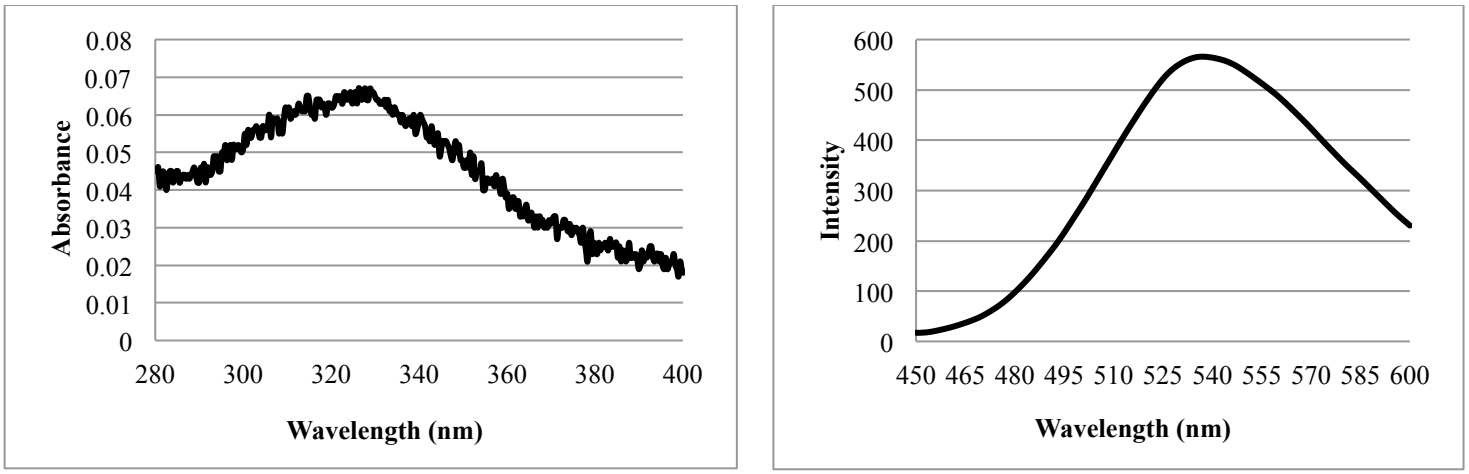


**Figure 21: Absorbance (left) and emission (right) spectra of 10 µM D2 in 10 mM PB pH 7.4**

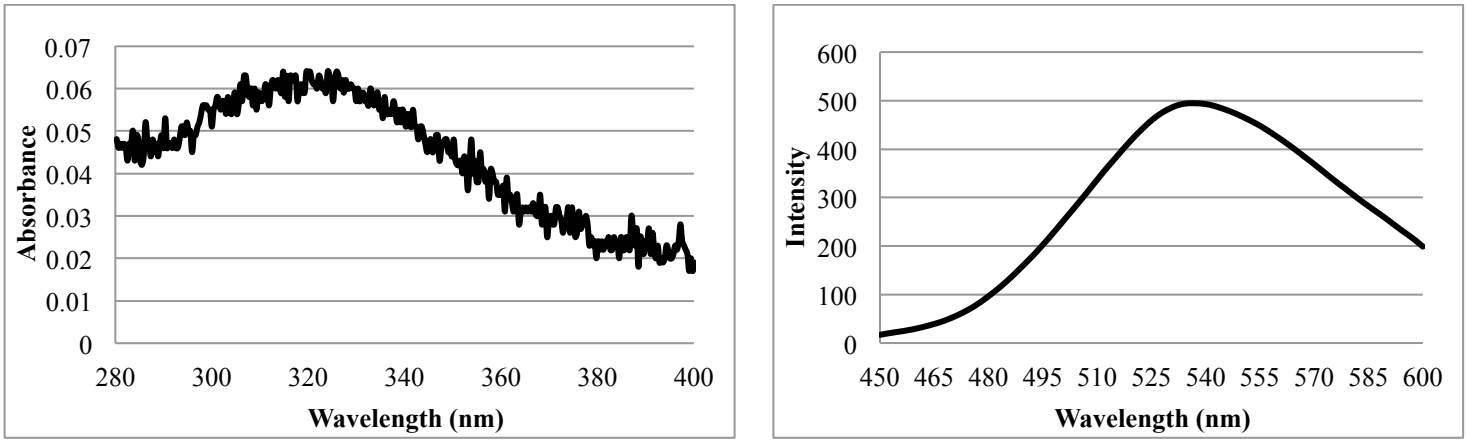


**Figure 22: Absorbance (left) and emission (right) spectra of 10 µM D-GSH in 10 mM PB pH 7.4**

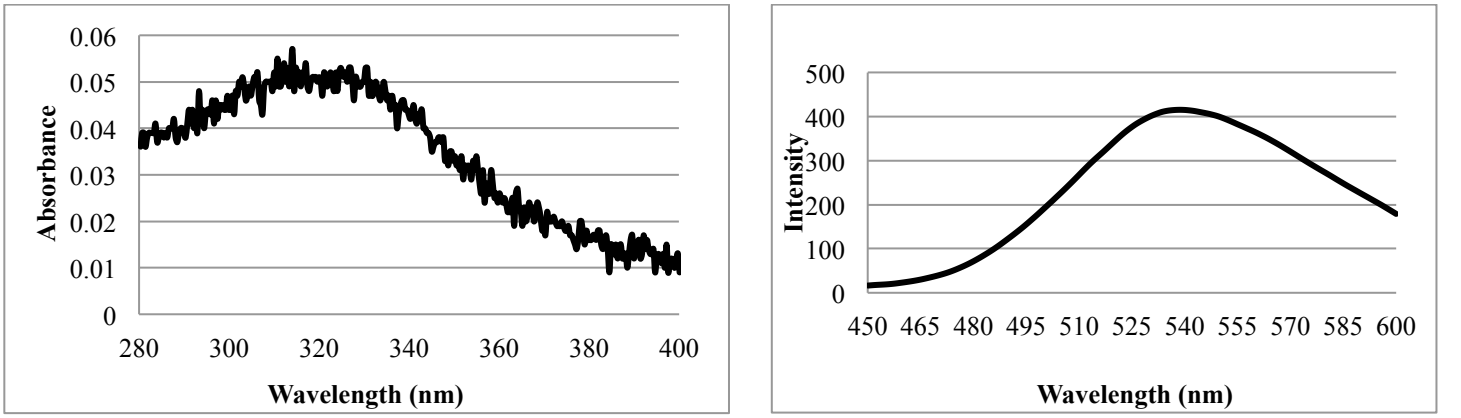


**Figure 23: Absorbance (left) and emission (right) spectra of 10 µM D-GSH + DTT in 10 mM PB pH 7.4**

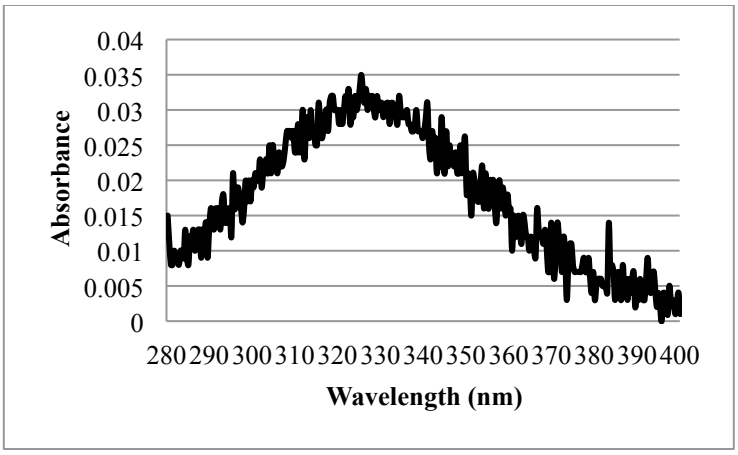


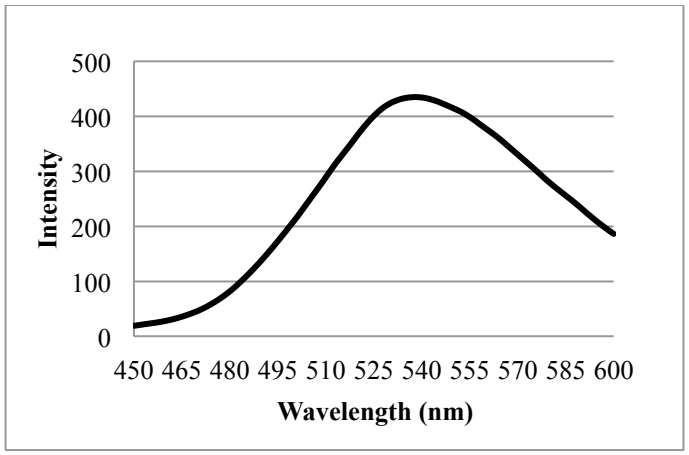


**Figure 24: Absorbance (left) and emission (right) spectra of 10 µM D-GSH + TCEP in 10 mM PB pH 7.4**

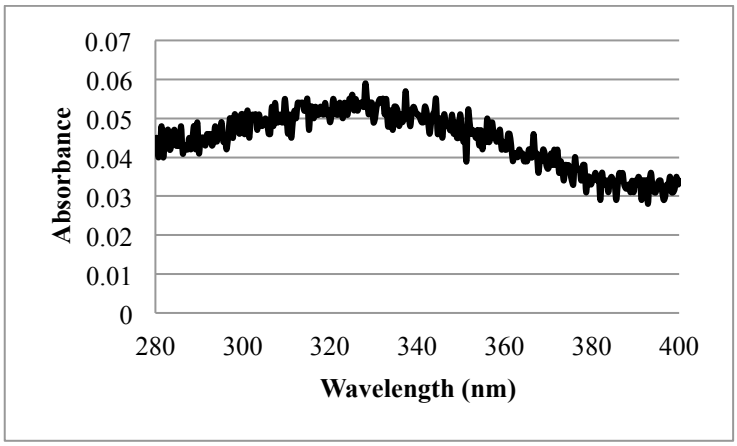


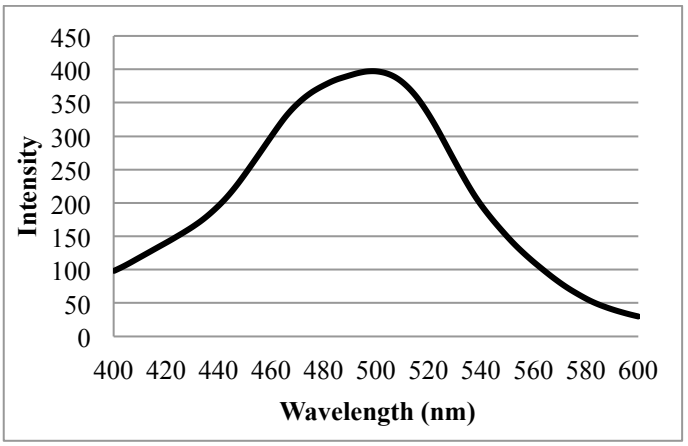


**Figure 25: Absorbance spectrum of 5.1 mM GS-DANS (left) and emission spectrum (right) of 10 uM GS-DANS in 10 mM PB pH 7.4**

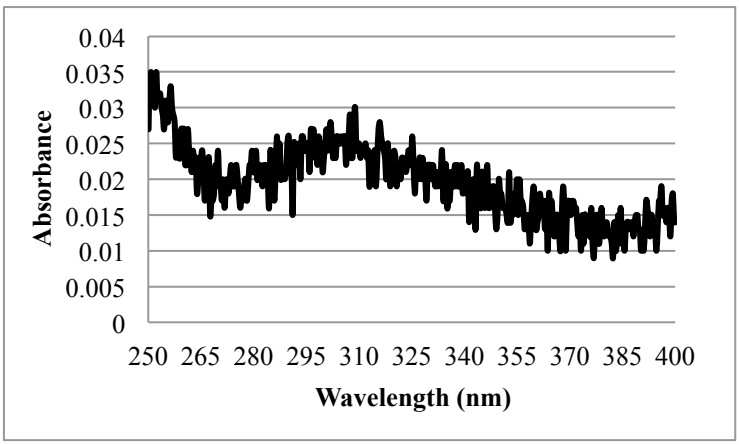


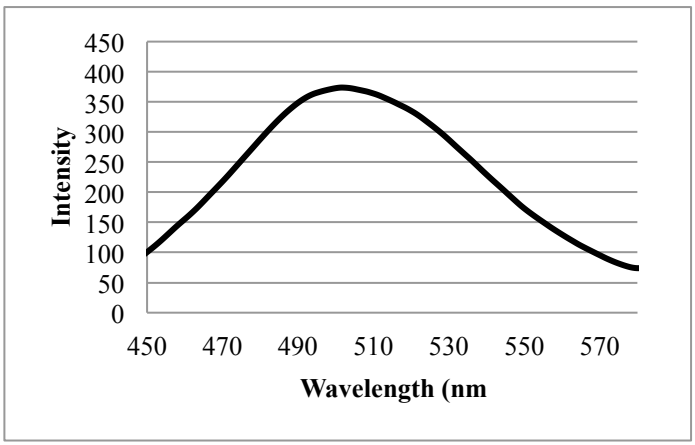


**Figure 26: Absorbance spectrum of 0.47 mM dansyl acid (left) and emission spectrum of 0.12 mM dansyl acid (right) in 10 mM PB pH 7.4**

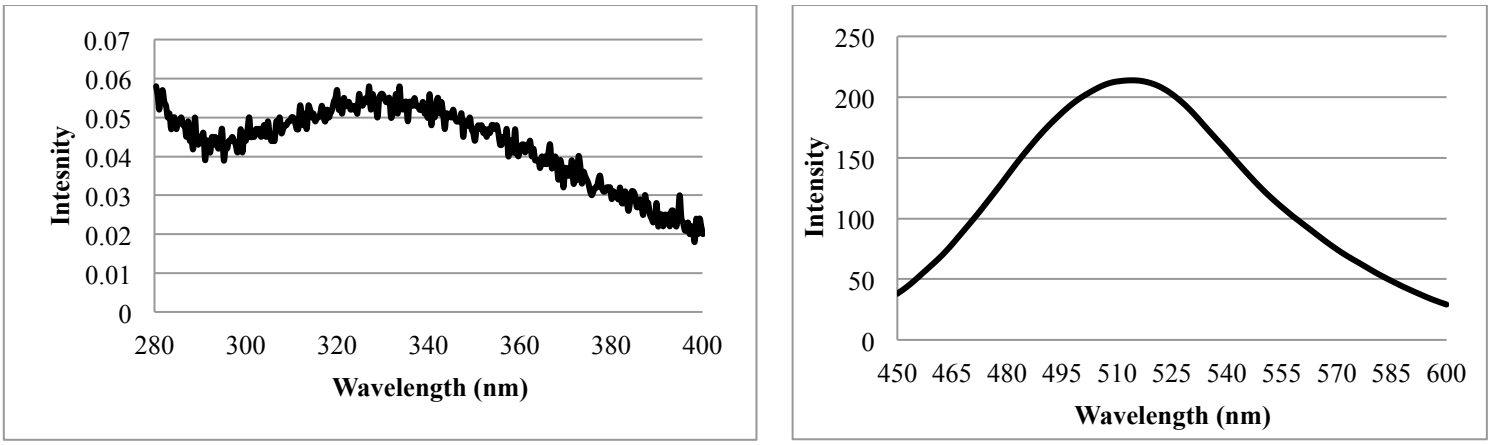


**Figure 27: Absorbance (left) and emission (right) spectra of 10 µM D-BSA in 10 mM PB pH 7.4**

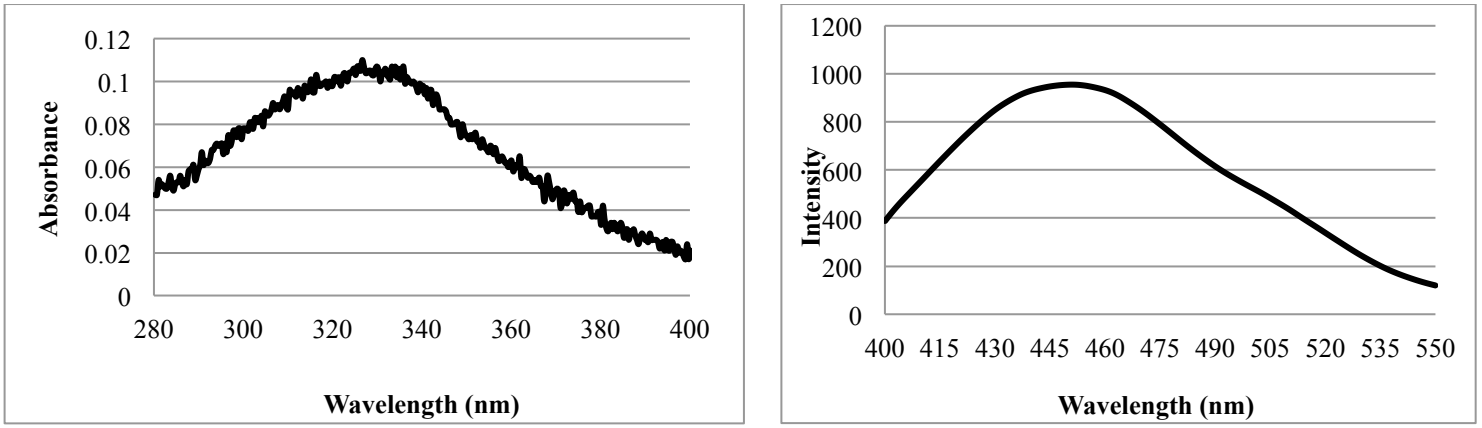


**Figure 28: Absorbance spectrum of 0.38 mM BSA-DANS (left) and emission spectrum of 810 nM BSA-DANS (right) in 10 mM PB pH 7.4**

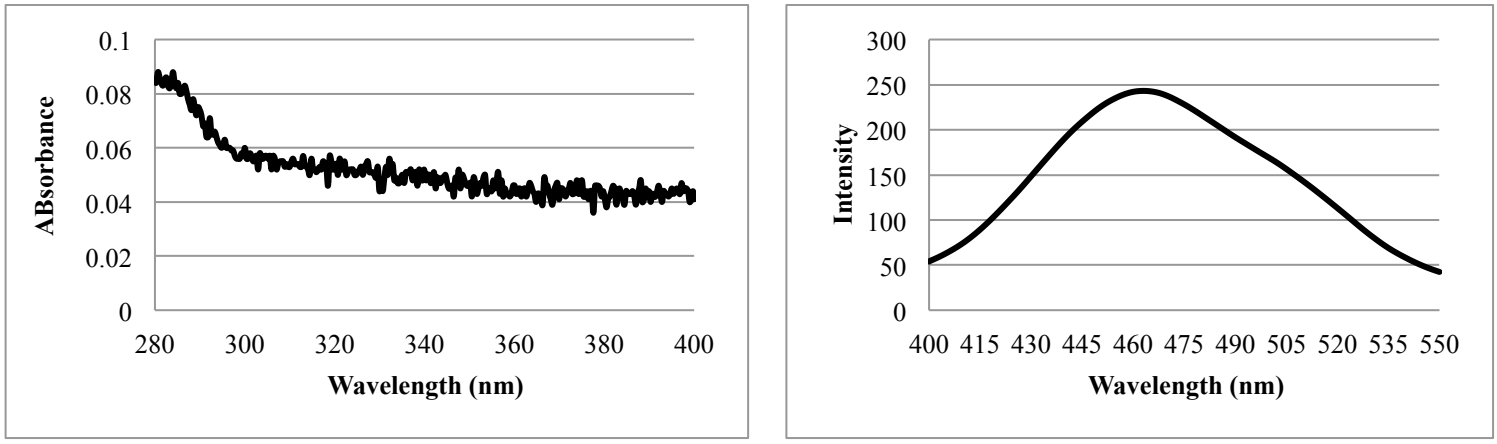


**Figure 29: Absorbance spectrum of 50 µL/mL EtOH-precipitated BSA-DANS (left) and emission spectrum of 10 µL/mL EtOH-precipitated BSA-DANS (right) in 10 mM PB pH 7.4**

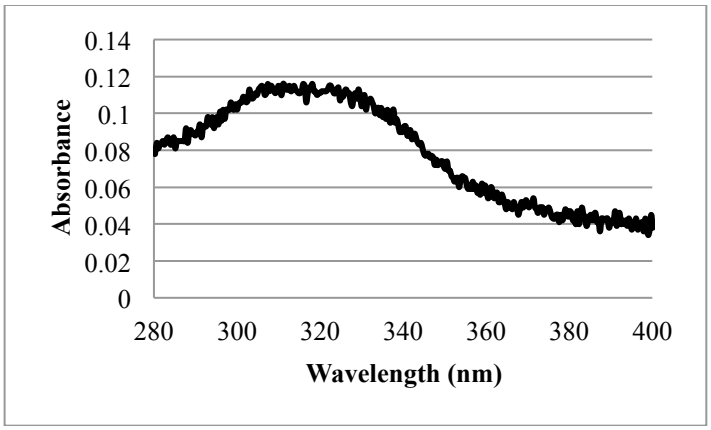


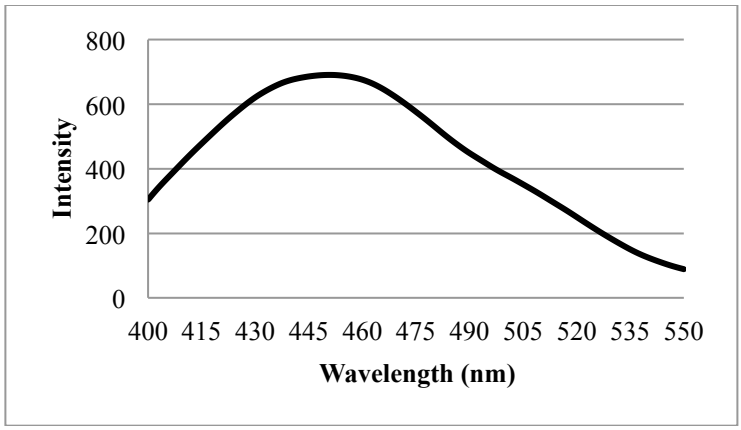


**Figure 30: Absorbance spectrum of 50 µL/mL BSA-DANS + 6% guHCl (left) and emission spectrum of 1 µL/mL BSA-DANS + 6% guHCl (right) in 10 mM PB pH 7.4**

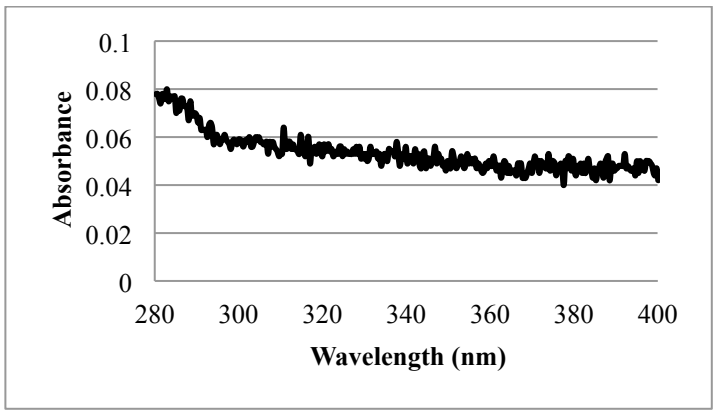


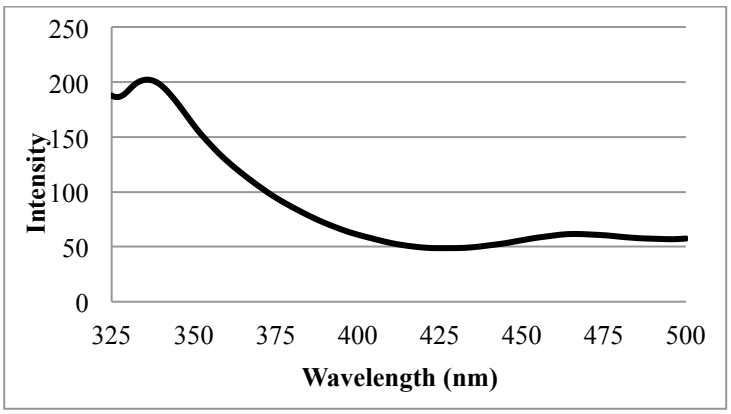


**Figure 31: Absorbance spectrum of 50 µL/mL SDS PAGE purified BSA-DANS (left) and emission spectrum of 10 µL/mL BSA-DANS (right) in 10 mM PB pH 7.4**

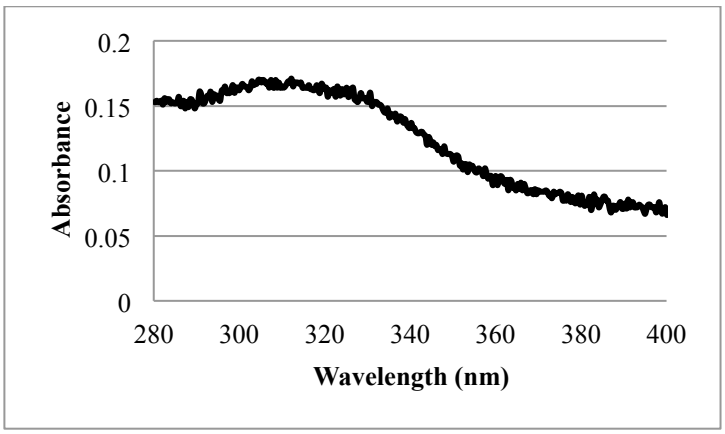


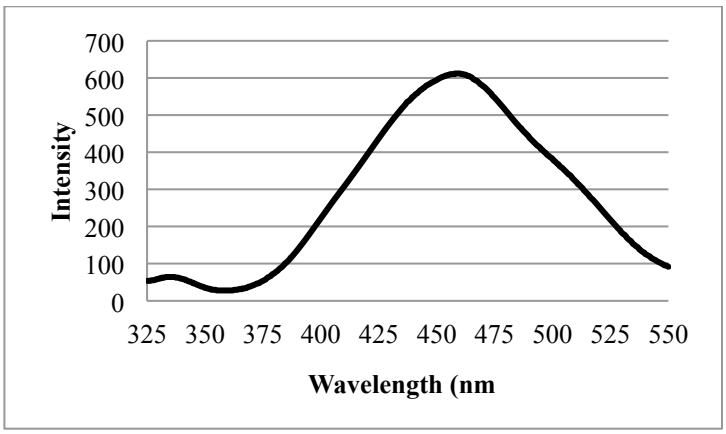


**Figure 32: Absorbance spectrum of 50 uL/mL BSA-DANS + 0.1 % SDS (left) and emission spectrum of 2 uL/mL BSA-DANS + 0.1% SDS (right) in 10 mM PB pH 7.4**

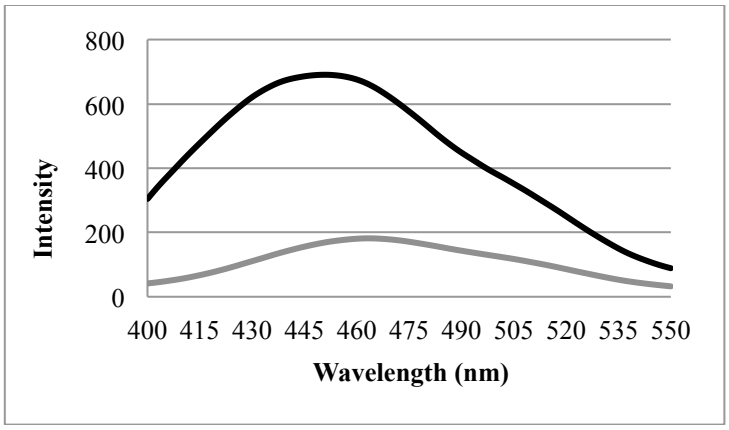


**Figure 33: Emission spectra of EtOH-precipitated BSA-DANS (grey) and BSA-DANS + 6% guHCl (black)**

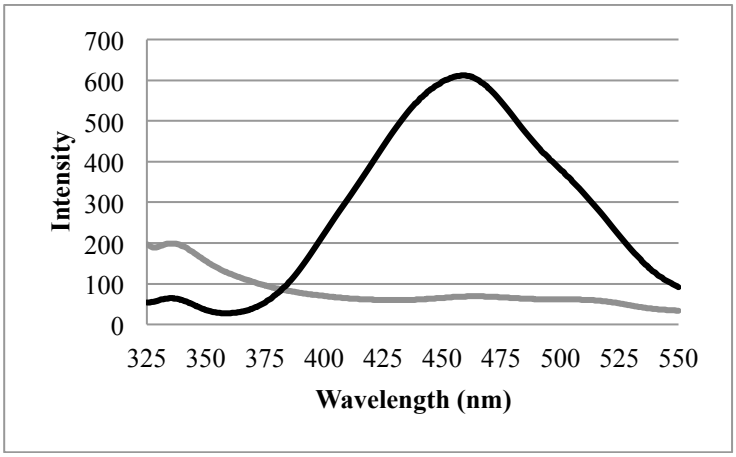


**Figure 34: Emission spectra of 10 uL/mL SDS PAGE purified BSA-DANS (grey) and 2 uL/mL BSA-DANS + 0.5% SDS (black)**

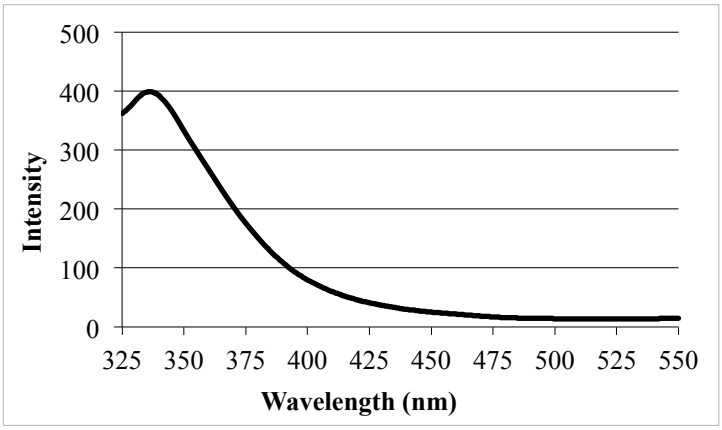


**Figure 35: Emission spectrum of 25 uL/mL BSA+SDS (1 mg/mL BSA + 0.5% SDS) in 10 mM PB pH 7.4**

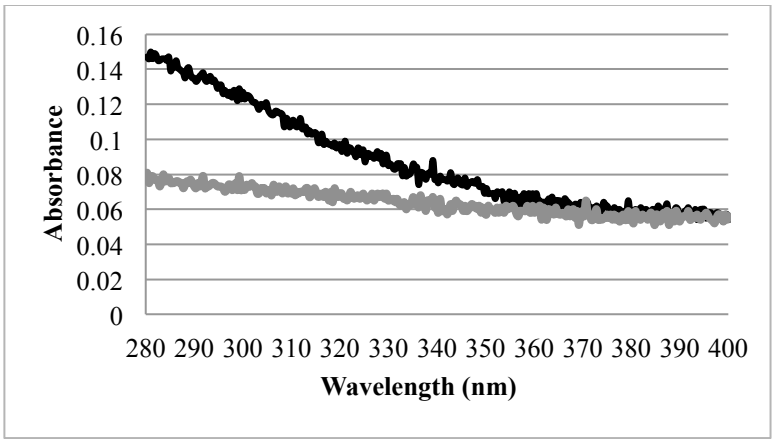


**Figure 36: Absorbance spectra of 1% SDS from LML (black) and from CJA (grey) in 10 mM PB pH 7.4**

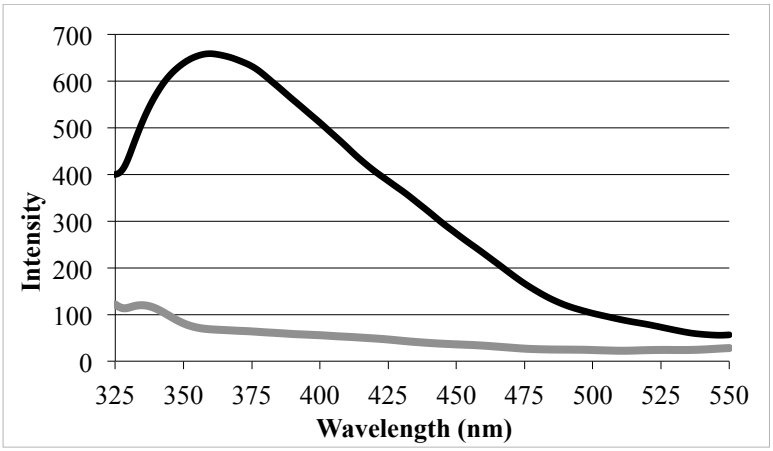


**Figure 37: Emission spectra of 1% SDS from LML (black) and from CJA (grey) in 10 mM PB pH 7.4**

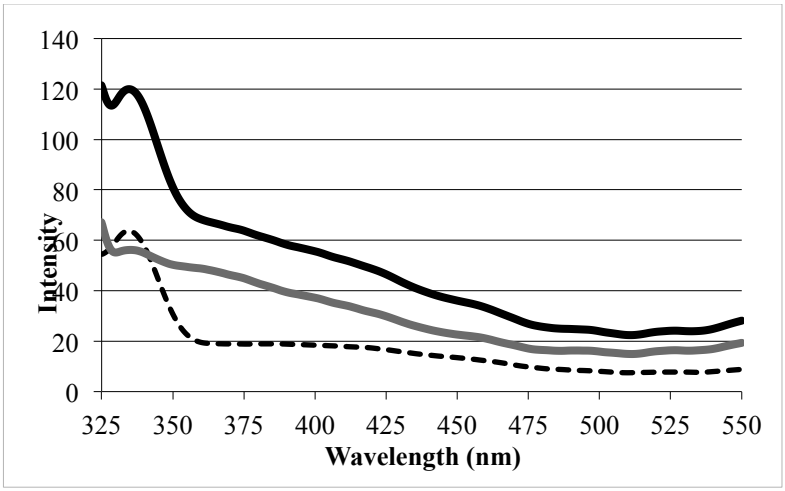


**Figure 38: Emission spectra of 1% SDS from CJA (black), 90% 10 mM PB pH 7.4 (dashed), and 1% SDS from CJA blanked (grey) in 10 mM PB pH 7.4**

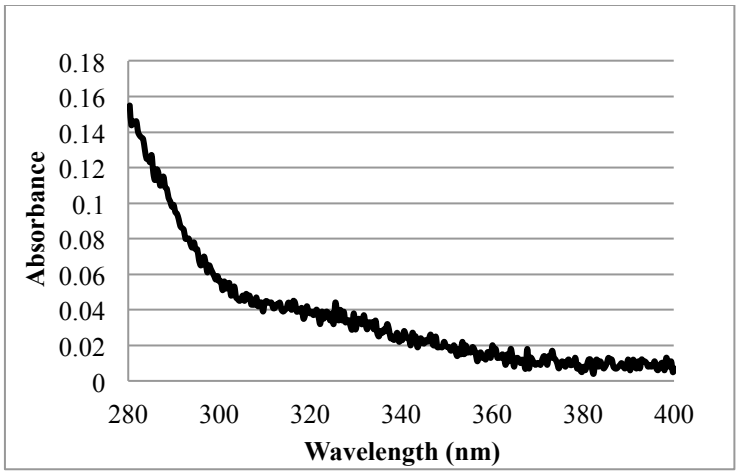


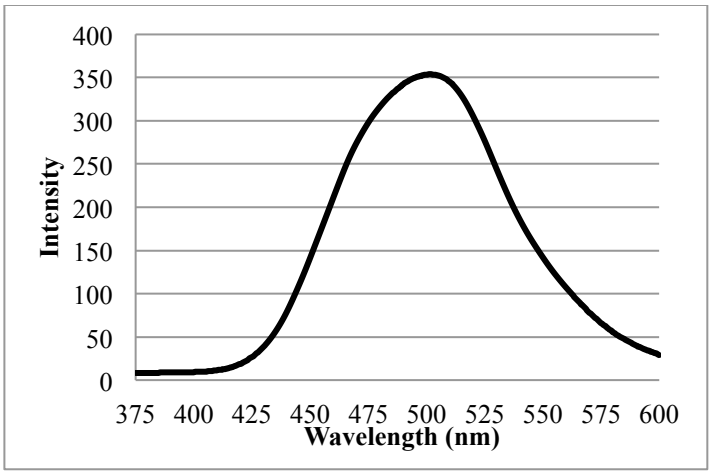


**Figure 39: Absorbance spectrum of 860 nM D-papain (left) and emission spectrum of 86 nM D-papain (right) in 10 mM PB pH 7.4**

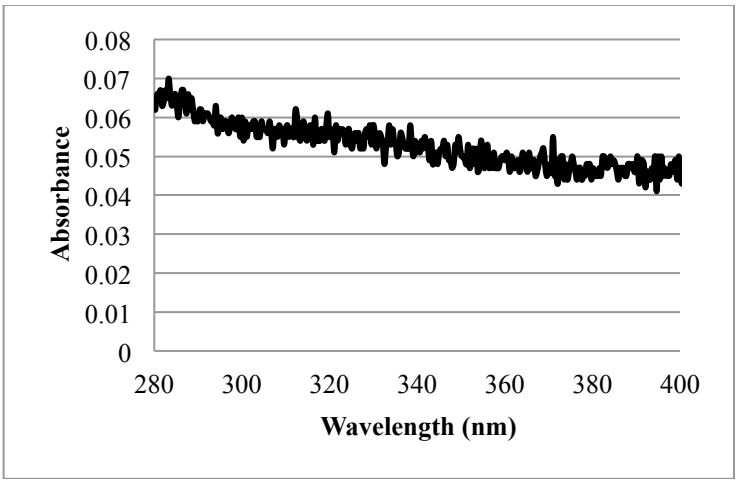


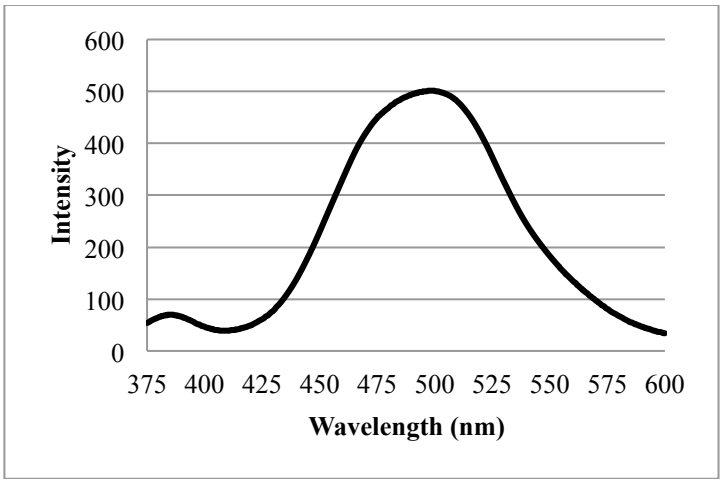


**Figure 40: Absorbance spectrum of 290 nM papain-DANS (left) and emission spectrum of 230 nM papain-DANS (right) in 10 mm PB pH 7.4**

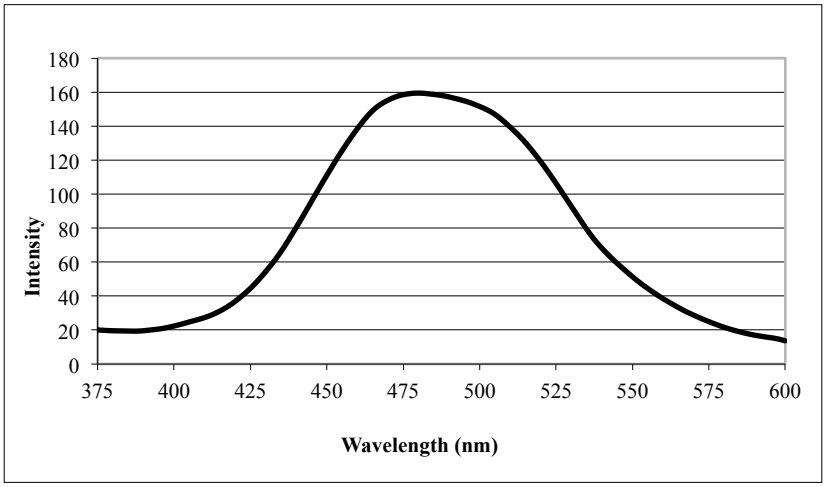


**Figure 41: Emission spectrum of 100 µL/mL EtOH-precipitated papain-DANS in 10 mM PB pH 7.4**